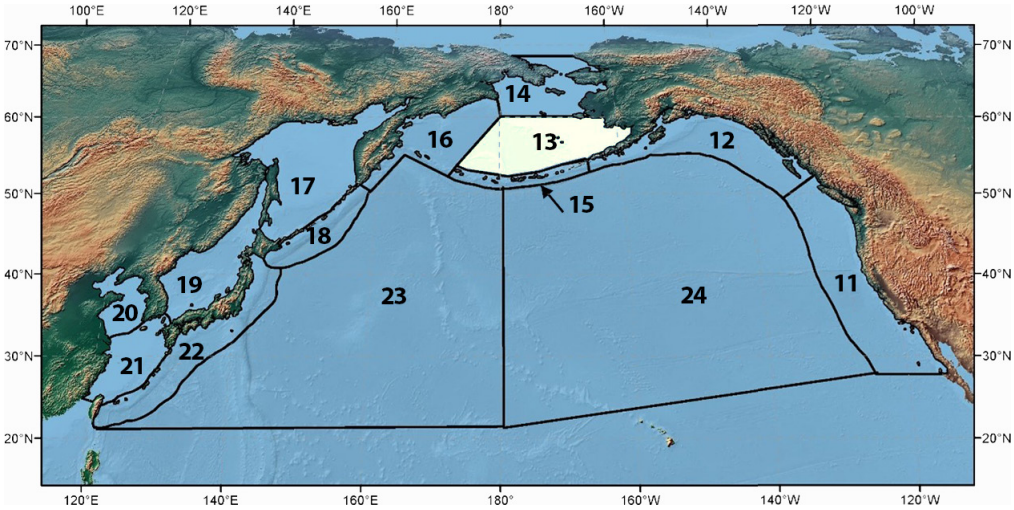

PICES

Regional Report for PICES Region: 13

PICES SPECIAL PUBLICATION 7

Marine Ecosystems of the North Pacific Ocean 2009–2016

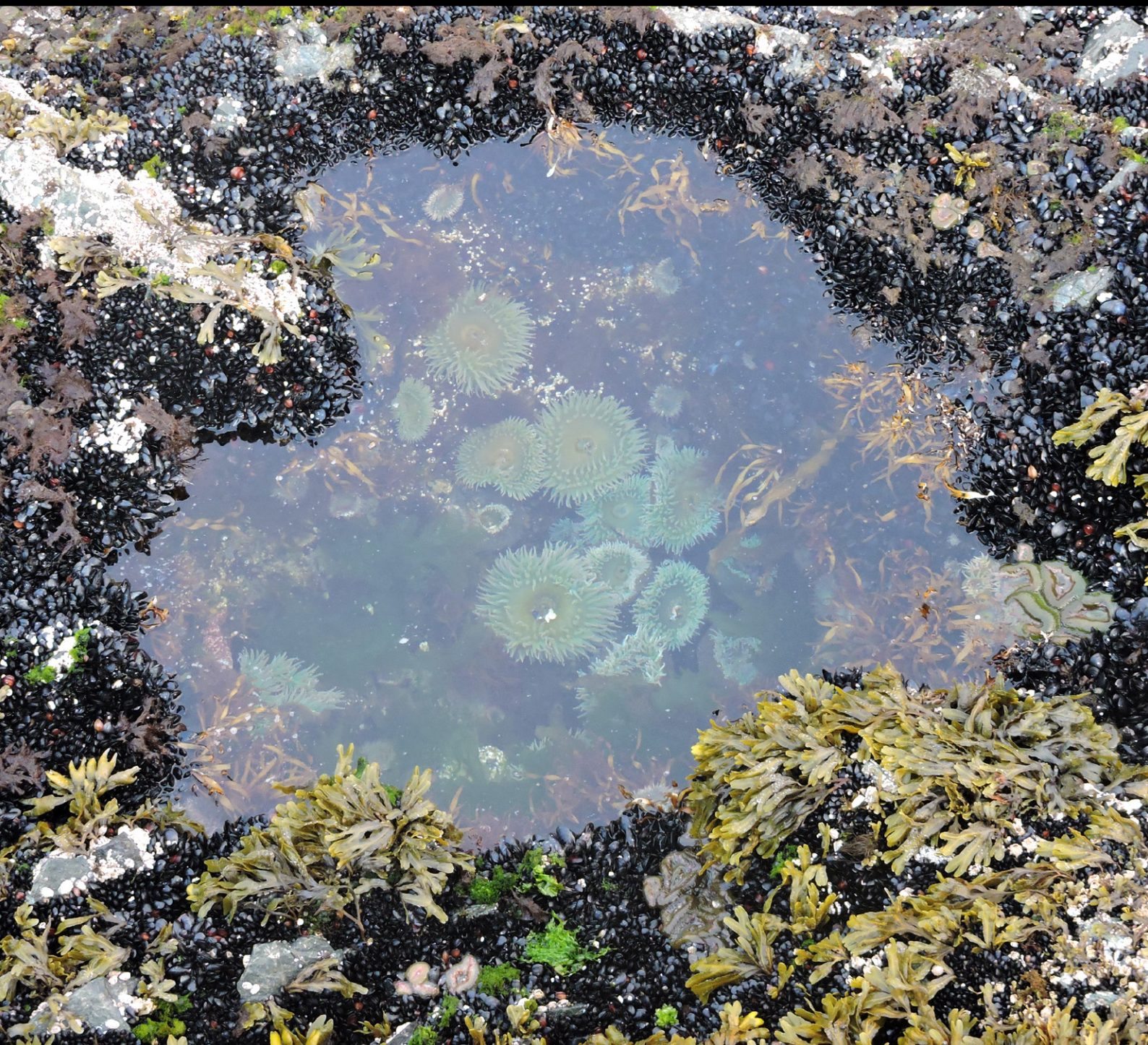

PICES North Pacific Ecosystem Status Report, Region 13 (Southeastern Bering Sea)

Elizabeth C. Siddon
NOAA Fisheries, Alaska Fisheries Science Center
Juneau, Alaska, USA

Contributors: Alex Andrews, Sonia Batten, John Bengtson, Jennifer Boldt, Nicholas Bond, Gregory Buck, Kristin Cieciel, Curry Cunningham, Elizabeth Dawson, Andrew Dimond, Sherri Dressel, Lisa Eisner, Nissa Ferm, Robert Foy, Corey Fugate, Jeanette Gann, Colleen Harpold, Jordan Head, Jerry Hoff, David Kimmel, Carol Ladd, Jesse Lamb, Christie Lang, Robert Lauth, Franz Mueter, Jim Murphy, James Overland, Rolf Ream, Heather Renner, Patrick Ressler, John Richar, Chris Rooper, Marc Romano, Sigrid Salo, Katie Sechrist, Elizabeth Siddon, Jeremy Sterling, Rod Towell, Jordan Watson, Michael Williams, Ellen Yasumiishi, and Stephani Zador

1. Highlights

The southeastern Bering Sea experienced cold oceanographic conditions between 2007–2013; 2014 was the beginning of a new warm stanza that persisted through late summer 2016. Therefore, the 5-year period from 2009-2014 encompassed an ecosystem-wide transition from below-average to above-average thermal conditions. The impact of this transition was observed at multiple trophic levels within the southeastern Bering Sea.

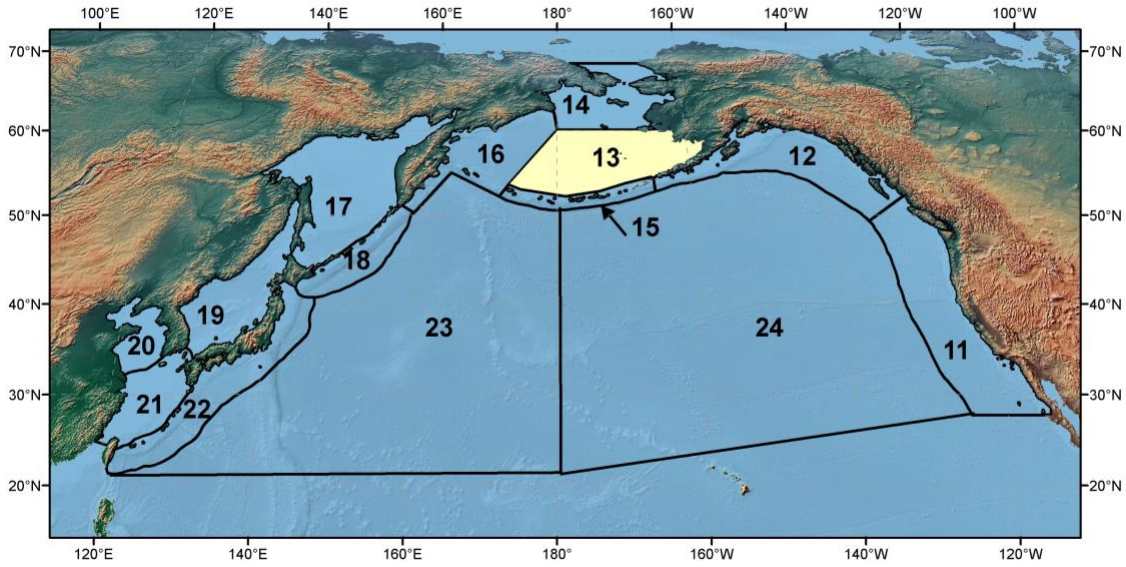

Figure R13-1. The PICES biogeographical regions and naming convention for the North Pacific Ocean with the area discussed in this report highlighted.

The southeastern Bering Sea had extensive sea ice and early spring blooms during 2009 through 2012; these conditions were favorable for lower trophic level production with moderately high concentrations of euphausiids and large copepods for planktivorous feeders. Increased productivity and the persistent cool conditions contributed to increased

year-class strength for fishes. For example, conditions were favorable for the overwinter survival of juvenile Walleye pollock (*Gadus chalcogrammus*; hereafter 'pollock') and Pacific cod (*Gadus macrocephalus*).

Jellyfish, primarily *Chrysaora melanaster*, first seen during the summer and fall of 2009, persisted through summer 2010 and increased in summer 2011. A previous episode of increasing jellyfish biomass was linked to a period of climatic transition from warm to moderate conditions, with a sharp decline in biomass at the transition back to a period of very warm conditions. Top-down control shaped the ecosystem, particularly with an increase in Arrowtooth flounder (*Atheresthes stomias*).

Climatic conditions moderated in 2011 with warmer bottom temperatures and less extensive maximum sea ice and cold pool (summer footprint of sea ice the preceding winter) extent. However, sea surface temperatures were much lower than average, reflecting the unusually cold atmospheric conditions during that summer. The cool summer contributed to the continuation of multi-year sequential cold ocean temperatures, which in 2012 included the most extensive cold pool area in recent history and the latest ice retreat (along with 2009) in more than two decades.

While cold conditions in the southeastern Bering Sea are typically associated with improved nutritional status of juvenile pollock prior to winter, 2012 demonstrated that conditions can be too cold to support good survival. In 2012, the pollock were energetically dense, as is usual in cold years, but with the combination of small size, the average energy content per fish was low. In contrast to biomass trends, length-weight residuals, an indicator of groundfish condition, were negative in 2012 for all examined species but Yellowfin sole (*Limanda aspera*). Groundfish condition is considered to be linked to ecosystem productivity, suggesting lower ecosystem productivity in 2012.

2014 broke the sequence of seven years with cold winter-spring temperatures (2007-2013), which had followed seven warm years (2000-2006). Spring 2014 near-surface air temperature anomalies in the southeastern Bering Sea were +2°C, in contrast to 2013 at -2.5°C and 2012 at -3°C; sea ice maximum extent was also reduced.

In the pelagic zone, euphausiid abundance continued a decline since a peak in abundance was observed in 2009. This suggested that foraging conditions for euphausiid predators were more limited in this year. Length-weight residuals, an indicator of fish condition, for juvenile pollock were strongly positive, similar to those during the warm years of 2002-2005, and indicative of good foraging conditions. Colder later summers during the late juvenile phase followed by warmer spring temperatures during the age-1 phase, as occurred in 2013-2014, are assumed favorable for the survival of pollock, further supporting that the 2013 pollock year class experienced favorable conditions in 2014. In general, the shift from sequential cold years to a warm year appeared to coincide with a surge in productivity for groundfish and seabirds as indicated by general biomass trends, groundfish condition, and seabird reproductive success.

2. Atmosphere

2.1. Climate Indices

Contributed by: Nicholas Bond
Joint Institute for the Study of the Atmosphere and Ocean (JISAO)
Box 354925, University of Washington, Seattle, WA 98195-4925

NINO3.4 – This index represents the normalized SST anomalies in the east-central tropical Pacific (5˚S – 5˚N; 170 -120˚W) and is used to summarize the state of the El Niño-Southern Oscillation (ENSO). Positive values of +1 and greater signify El Niño events; negative values signify La Nina. ENSO neutral conditions are assumed to be present when the magnitude of NINO3.4 is less than 0.5 to 1, depending on the application and averaging period. ENSO generally has its strongest expression during the boreal winter, which is also the time of year when it has more robust connections to the atmospheric circulation of the North Pacific Ocean. El Niño and La Nina events tend to be accompanied by relatively low and high sea level pressure (SLP), respectively, in the vicinity of the Aleutian low. The time series provided here is a three-month running mean of NINO3.4 monthly anomaly values in ˚C. This time series was produced from data at https://www.cpc.noaa.gov/data/indices/SSToi.indices, based on OISST.v2 data compiled by NOAA's Climate Prediction Center. Users of NINO3.4 and other SST-based climate indices should be aware that different SST analyses yield slightly different values for these indices. In addition, there are a host of ENSO indices with a variety of atmospheric and oceanic variables as inputs. The discrepancies between ENSO indices are usually minor with respect to characterization of the major fluctuations in ENSO.

Trends: ENSO exhibits periodicity on time scales typically of 2 to 7 years. The period of interest here (2009 into 2019) featured the following prominent events: a moderately strong El Niño during the boreal winter of 2009-2010, La Nina conditions during the winter of 2010-11, and to a lesser extent during the winter of 2011-12, and an intense El Niño that developed during summer 2015 and persisted into the spring of 2016. The tropical Pacific was also warmer than normal during the previous winter of 2014-15; in some classification systems it qualifies as an El Niño winter and in others it does not. Similarly, the tropical Pacific was cooler than normal during the winters of 2016-17 and 2017-18, and warmer than normal during the winter of 2018-19, with all three periods representing borderline ENSO events.

Pacific Decadal Oscillation (PDO) – The PDO represents the leading mode of variability in North Pacific SST. It was first related to western North America salmon catches (Mantua et al. 1997) and since linked to a host of marine ecosystem variations. The PDO responds to the strength of the Aleutian low (Newman et al. 2016), with upper-ocean processes and thermal inertia serving to low-pass filter the atmospheric forcing. Monthly values of the PDO in normalized form are available at the following website: https://oceanview.pfeg.noaa.gov/erddap/tabledap/cciea_OC_PDO.htmlTable?time,PDO. These data were used to form the three-month running means included here.

Trends: The PDO was in a mostly negative state from 2008 through 2013, with a short period of weakly positive values from late 2009 into 2010 (the annual averaged PDO for these two years was less than zero). A marked shift in the PDO began in late 2013 with positive values for this index prevailing from 2014 into 2017. This increase can be attributed initially to the development of the NE Pacific marine heat wave of 2014-16,

and was reinforced by the atmospheric forcing associated with El Niño during the winter of 2015-16, in particular a deeper than normal Aleutian low. The PDO was mostly near zero from late 2017 through late 2018 and became positive in 2019.

North Pacific Index (NPI) – The NPI is used to characterize the strength of the Aleutian low, specifically the area-weighted sea level pressure (SLP) in hPa over the region of 30 - 65˚N, 160˚E – 140˚W (Trenberth and Hurrell, 1994). Perhaps it best serves as an atmospheric circulation index for the North Pacific during the boreal winter in that it often but not strictly relates to the state of ENSO. During summer, positive (negative) values of the NPI can also reflect an enhanced (suppressed) or northwestward (southeastward) displaced North Pacific High. The three-month running mean NPI time series shown here was produced using SLP data from the NCEP Reanalysis available at the following website: https://www.esrl.noaa.gov/psd/dat/climateindices.

Trends: The NPI is an atmospheric index and therefore has inherently greater high-frequency variability than most oceanic indices. For the winters considered here, it was negative in 2009-10 and 2015-16 during periods of El Niño. Note that the former event was substantially weaker than the latter event as gauged by the NINO3.4 index, but that the remote atmospheric responses in terms of the NPI were comparable. The weak to moderate La Ninas of 2010-11, 2011-12, 2016-17 and 2017-18 were accompanied by positive states of the NPI. There were other winters during which the NPI was positive but lacking a connection to ENSO. Note that positive (negative) values for the NPI tend to correspond with negative (positive) states in the PDO on multi-year time scales. The NPI generally exhibits less variance in summer than in winter, but substantial positive values for this index were observed in the summers of 2016 and 2018. The upshot was a suppression in storminess and low clouds which served to help maintain the warmer than normal upper ocean temperatures in the Gulf of Alaska and Bering Sea that developed in 2014.

North Pacific Gyre Oscillation (NPGO) – The NPGO represents the second leading mode of sea surface height (SSH) variability in the North Pacific. Di Lorenzo et al. (2008, among later articles) have shown that the NPGO is related to a variety of physical and biochemical ocean variables in the eastern North Pacific. Kilduff et al. (2015) show that recent salmon runs along the US west coast exhibit greater correspondence with the NPGO than the PDO. The NPGO has also been related to zooplankton species composition in the western North Pacific (Chiba et al. 2013). Three-month running means were formed from the monthly values of the NPGO in normalized form downloaded from the following website: http://www.o3d.org/npgo/.

Trends (Figure R13-2): Positive values of the NPGO prevailed from 2009 through most of 2013, implying relatively cool SST across the North Pacific north of about 40 N and warm SST in the western North Pacific south of 40 N. The NPGO shifted phase in late 2013 and declined more or less steadily to a strongly negative state during 2018. An exception was 2016, during which the NPGO was near neutral. This period of 2014-18 features relatively warm upper ocean temperatures in much of the northeast Pacific.

Arctic Oscillation (AO) – The AO represents a measure of the strength of the polar vortex, with positive values signifying anomalously low pressure over the Arctic and high pressure over the Pacific and Atlantic Ocean at a latitude of roughly 45ºN. During positive states of the AO, the southeast Bering Sea tends to experience fewer winter storms of mid-latitude/maritime origin and hence also tends to be slightly cooler than

normal. This relationship is weak, however, in that similar values of the AO can be accompanied by north-south wind anomalies, and hence air temperature anomalies, of either sign. Data considered here is from the following website: https://www.cpc.ncep.noaa.gov/products/precip/CWlink/daily_ao_index/monthly.ao.index.b50.current.ascii.table

Trends: The AO underwent relatively large and long-lasting shifts between negative and positive from 2009 into 2013, with a particularly large negative value during the winter of 2009-10 and positive values during early and late 2011. The AO has been more positive than negative in an overall sense during the period of 2014 through 2018, with short-term fluctuations between positive and near-neutral values.

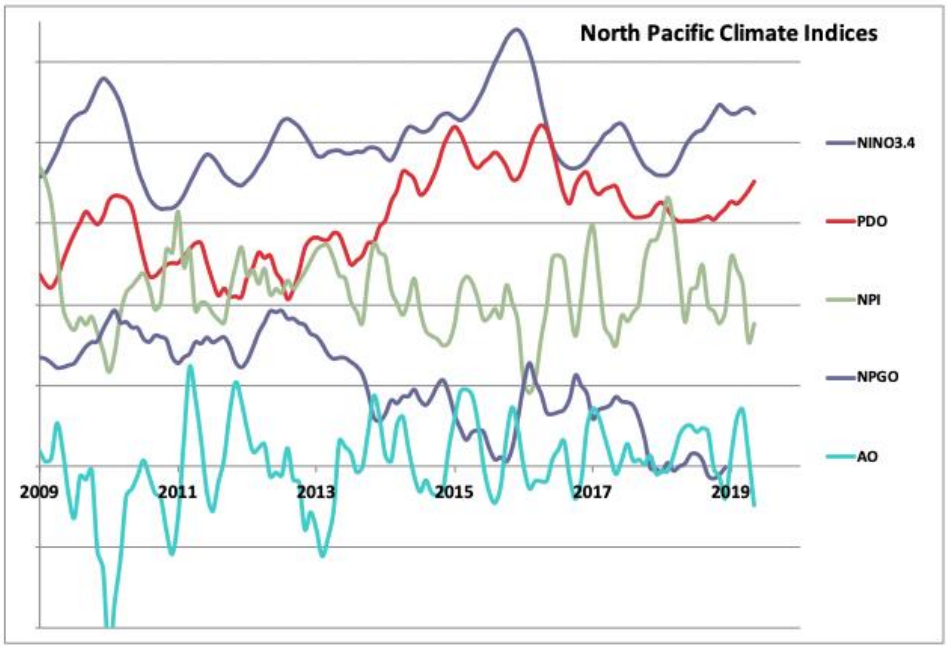

Figure R13-2. North Pacific Climate indices from 2009 to 2019.

3. Physical Oceanography

3.1. Air Temperature Anomalies at St. Paul Island

Contributed by: James Overland
NOAA/Pacific Marine Environmental Lab

Methods: St. Paul air temperatures are calculated from a National Weather Service standard observation station (57°09' N, 170°13' W).

Trends (Figure R13-3): Long-term surface air temperatures measured on St. Paul Island reflect the transition from cool anomalies during 2007–2013 to warm anomalies after 2014. The St. Paul temperature anomalies have been on the positive side (warm) since April 2014 for every single month. In 2018, four new records were set for the warmest temperature anomalies since 1980: February, March, April, and May 2018.

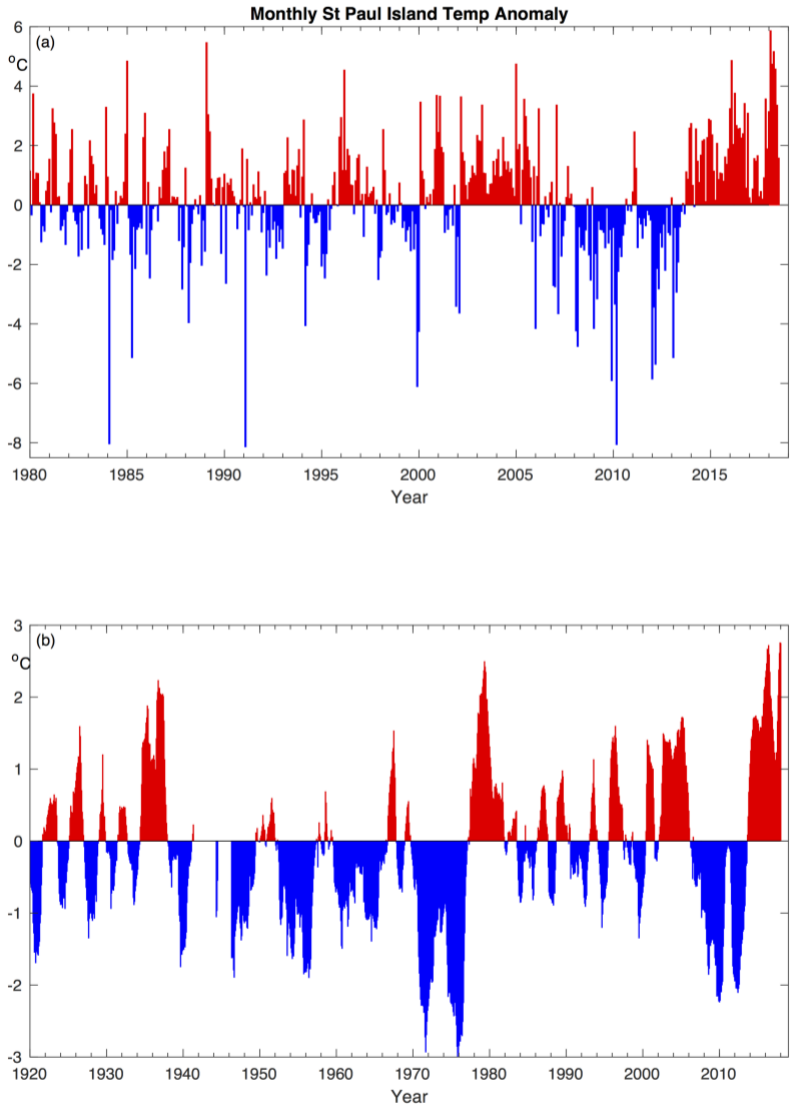

Figure R13-3. Mean monthly surface air temperatures anomalies at St. Paul (Pribilof Islands). (a) Unsmoothed 1980-2018 and (b) smoothed by 13-month running averages, January 1920 through August 2018. The base period for calculating anomalies is 1981-2010.

3.2. Cold Pool Extent

Contributed by: Carol Ladd
NOAA/Pacific Marine Environmental Lab

The cold pool, defined by bottom temperatures <2°C, influences not only near-bottom biological habitat, but also the overall thermal stratification and ultimately the mixing of nutrient-rich water from depth into the euphotic zone during summer.

Trends (Figure R13-4): A sequence of cool years, with larger cold pool extent, occurred from 2009-2013. The cold pool extent was small during 2014-2016, reflecting warm conditions and low ice cover extent during winter. In 2017, the cold pool extended over most of the middle shelf but was confined in the on-shelf/off-shelf direction. The summer 2018 cold pool extent was nearly non-existent, reflecting the very low sea ice extent the previous winter.

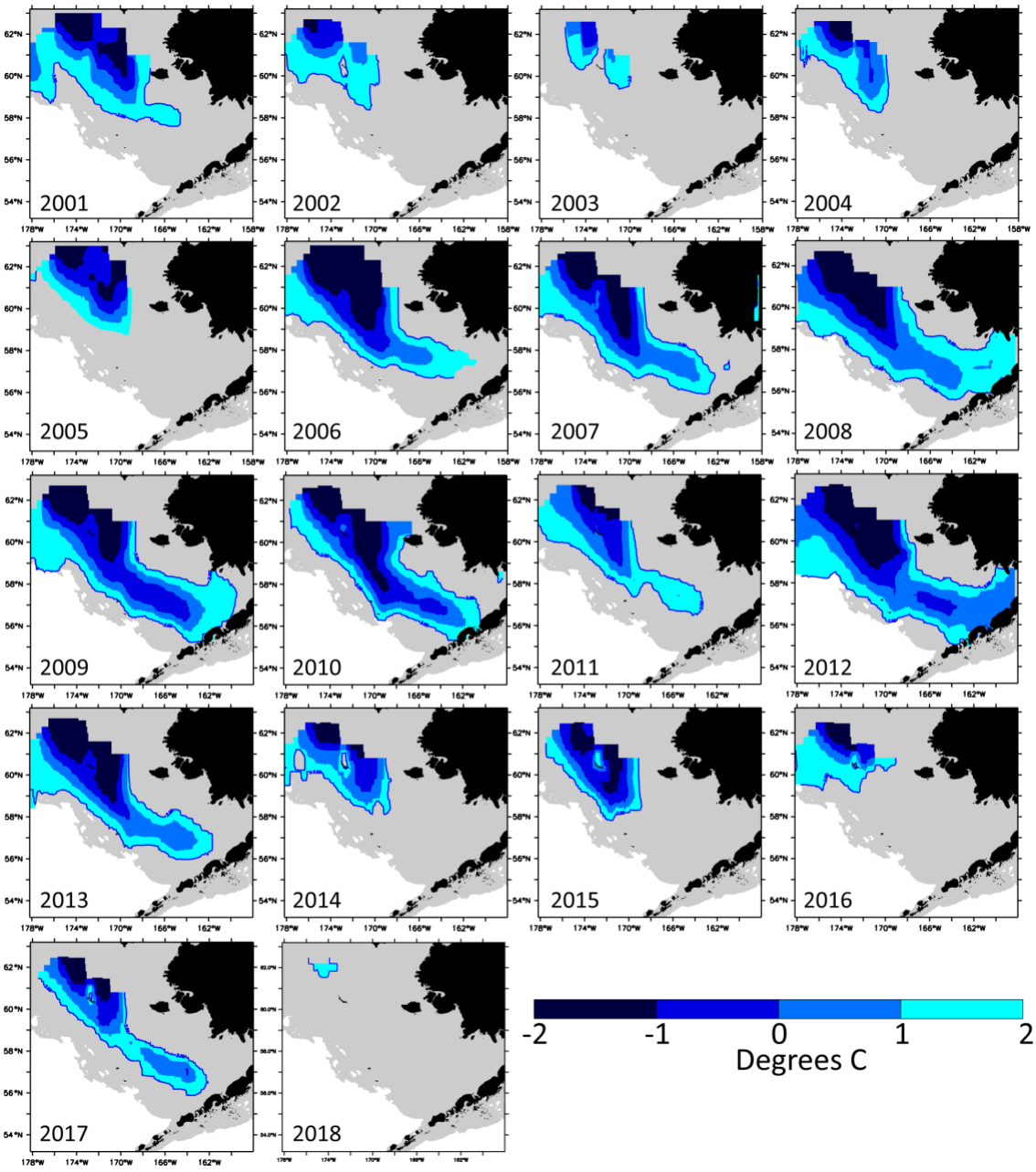

Figure R13-4. Cold pool (bottom temperatures <2°C) extent in the eastern Bering Sea (53°N-63°N, 160°W-178°W) from 2001-2018.

3.3. Satellite-derived Sea Surface Temperatures for Alaska Fishery Management Areas in the Bering Sea

Contributed by: Jordan Watson
NOAA/Alaska Fisheries Science Center

Methods: Using the NASA multi-scale ultra-high resolution (MUR) SST dataset, a combination of collection modalities creates a gap-free blend of sea surface temperature data (https://mur.jpl.nasa.gov/InformationText.php). Data are available at the daily level for the North Pacific from mid-2002 to present and can be downloaded from the NOAA Coast Watch West Coast Node ERDDAP server (https://coastwatch.pfeg.noaa.gov/erddap/) where they are searchable as “Multi-scale ultra-high resolution (MUR) SST Analysis fv04.1, Global, 0.01o, 2002-present, daily.” Data for this study were aggregated and summarized as described in Watson (2019).

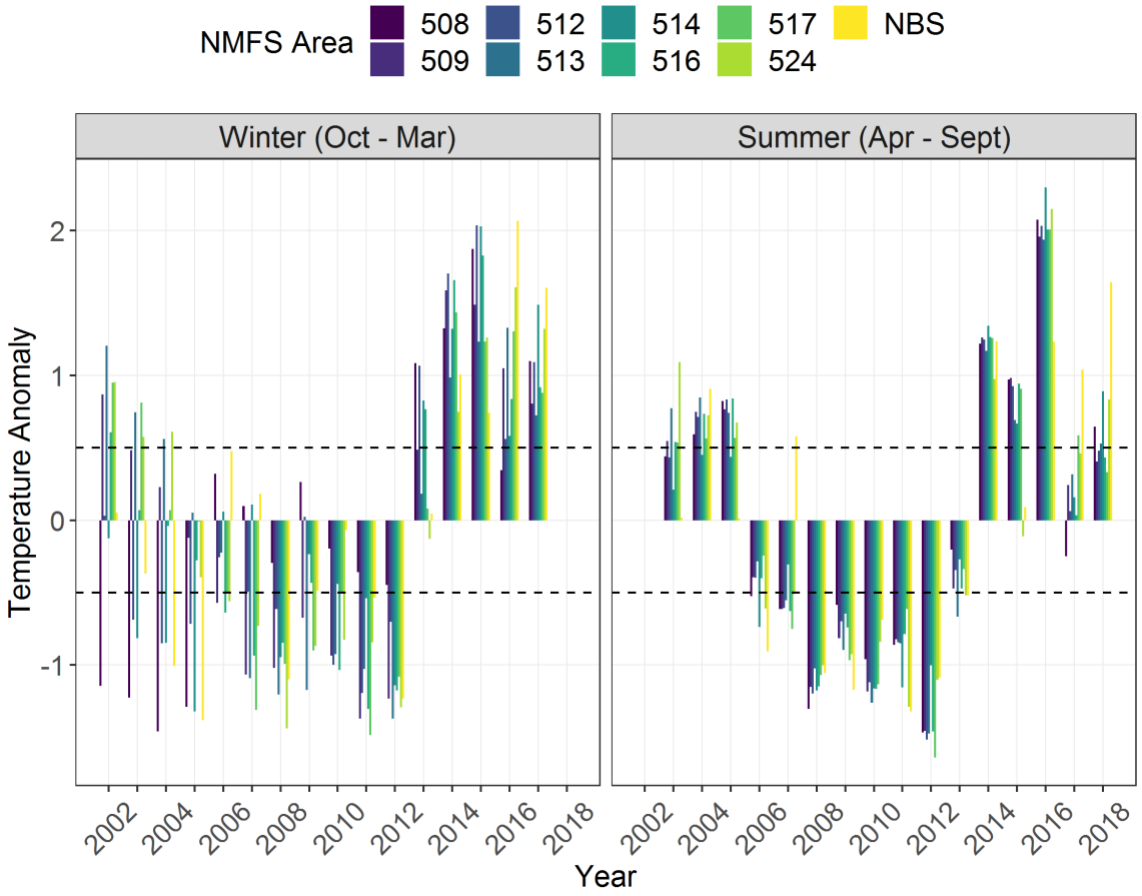

Figure R13-5: Seasonal sea surface temperature anomalies (C°) in the National Marine Fisheries Service (NMFS) areas for the Bering Sea. Data were unavailable for summer 2002 and winter 2018.

Trends (Figure R13-5): The satellite derived time series of summer sea surface temperatures demonstrates a general spatial coherence across the National Marine Fisheries Service (NMFS) areas and years. During winter, there was a greater degree of

spatial variability in temperature anomalies in the earlier years (when summer temperatures were anomalously warm) with some NMFS areas demonstrating negative anomalies and others revealing positive anomalies. Most notable is the transition from cold anomalies at the beginning of the 2009-2016 period to warm anomalies during the end of that period. The majority of the shift from warm to cold occurred during 2013, when summer temperatures were within half a degree of the 2002 – 2018 summer average, and winter temperatures (Oct 2013 – Mar 2014) for the more southern regions of the EBS were above average and northern Bering Sea temperatures hovered around the mean. In subsequent years, temperatures in the northern Bering Sea in particular have been among their warmest during both winter and summer.

3.4. Average Summer Surface and Bottom Temperatures

Contributed by: Robert Lauth
NOAA/Alaska Fisheries Science Center

Warm and cold years are the result of interannual variability in climatic conditions that affect the extent, timing, and retreat of sea ice on the eastern Bering Sea shelf. During warmer than average years, seasonal sea ice generally does not extend as far down the shelf and retreats earlier in the spring. The relatively large interannual fluctuations in bottom temperature on the eastern Bering Sea shelf affect the spatial and temporal distribution of groundfishes and the structure and ecology of the marine community. The timing of phytoplankton and subsequent zooplankton blooms are also affected by the extent of sea ice and timing of its retreat which in turn can affect survival and recruitment in larval and juvenile fishes as well as the energy flow in the system.

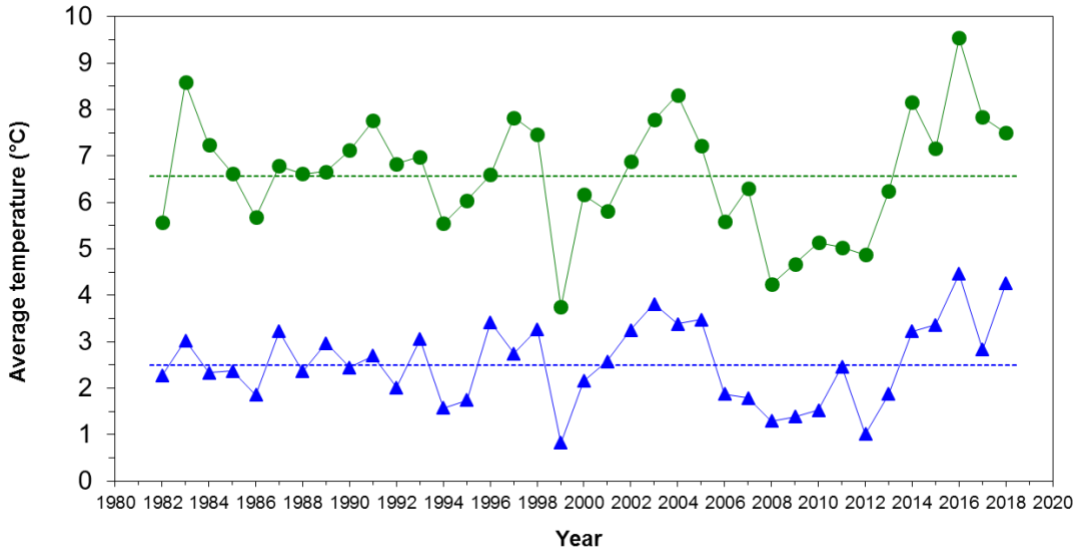

Figure R13-6: Average summer surface (green circles) and bottom (blue triangles) temperatures (°C) of the eastern Bering Sea shelf collected during the standard bottom trawl surveys from 1982-2018. Dotted lines represent the time-series mean for 1982-2018.

Trends (Figure R13-6): Surface and bottom temperature means for 2009-2013 were below average and both have remained above average since 2014. The 2018 surface temperature mean decreased from the 2017 estimate, while bottom temperature mean increased from the 2017 estimate, but both were still warmer than the long-term time-series mean.

4. Chemical Oceanography

4.1. Dissolved Inorganic Nitrogen Concentrations Above and Below the Pycnocline in the Eastern Bering Sea

Contributed by: Jeanette C. Gann and Lisa B. Eisner
NOAA/Alaska Fisheries Science Center, 17109 Pt Lena Loop Rd., Juneau, AK 99801

Methods: We viewed total dissolved inorganic nitrogen (DIN) concentrations (µM) above and below the pycnocline during late summer/early fall, 2003–2016 in the eastern Bering Sea. Data is divided by oceanographic inner domains (outer domain is left out due to inconsistent sampling) and further split between the northern and southern shelf at 60ºN. DIN (nitrate, nitrite, and ammonia) above the pycnocline at the surface mixed layer represent what is currently available for primary production at the end of summer (storm activity/wind mixing of deep nutrients to the surface tend to be lower during the summer, and surface nutrient stores are often depleted). Nutrients below the pycnocline represent what is potentially available should wind mixing become strong enough to break down the pycnocline and mix deeper layers to the surface. Sometime during autumn when wind storms increase in frequency and intensity, there is usually a second significant bloom of phytoplankton (though smaller than the spring bloom) after the summer pycnocline breaks down. During this time the deep nutrient stores are brought to the surface. This process is important for sending a new pulse of energy through the food web just prior to the onset of winter.

Trends: DIN both above and below the pycnocline varies from year to year over the eastern Bering Sea shelf in inner and middle domains. As expected, the inner domain, which is often thoroughly mixed from surface to deep, shows more correlation between the surface and deep waters (with significant correlation in the north ($P=0.002$), while in the middle domain there is considerably less correlation (Fig. R13-7). Also as expected, deeper stores of nutrients are usually found at higher concentrations than their surface counterparts. In addition, a significant decreasing trend is seen in surface DIN concentrations within the southern middle domain over time ($P<0.05$, Fig. R13-8).

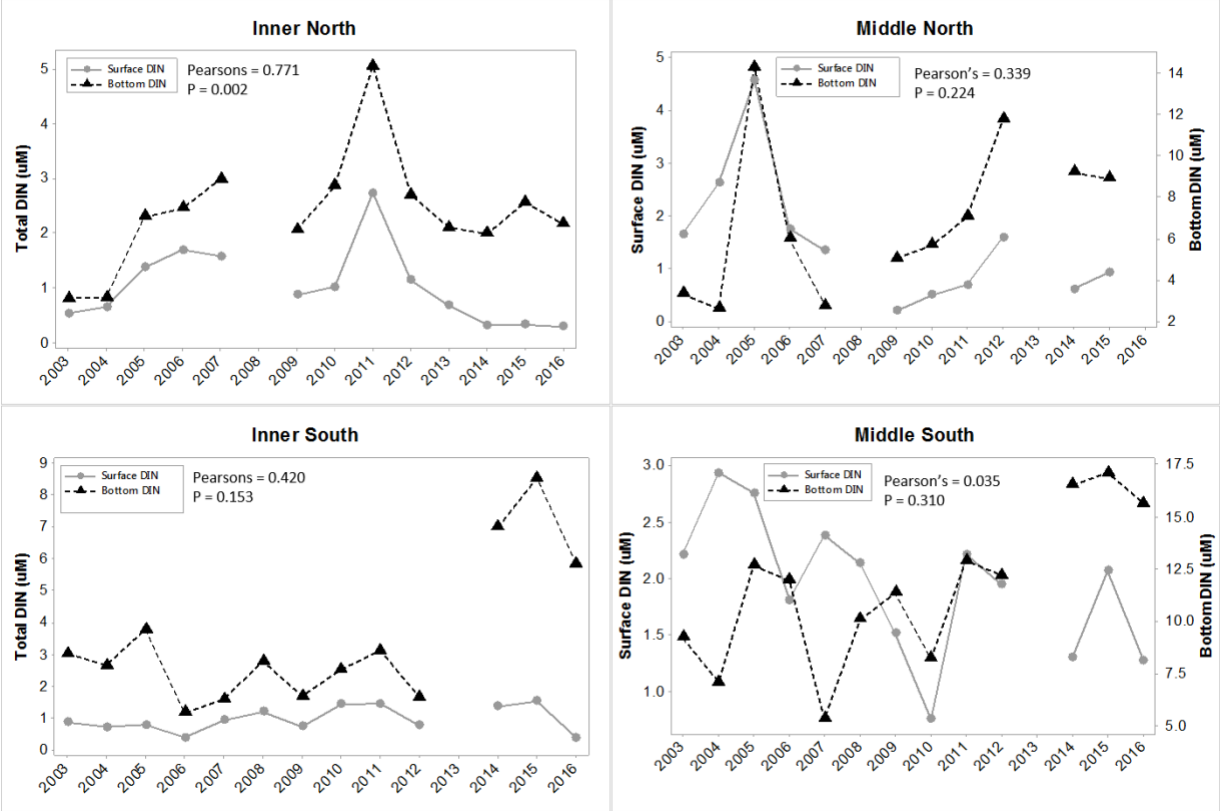

Figure R13-7. Mean total dissolved inorganic nitrogen concentrations (μM) above and below the pycnocline with Pearson's correlation coefficient (surface DIN vs bottom DIN) and P values shown (2003-2016). (Note the middle domain was not surveyed in the northern Bering Sea during 2016).

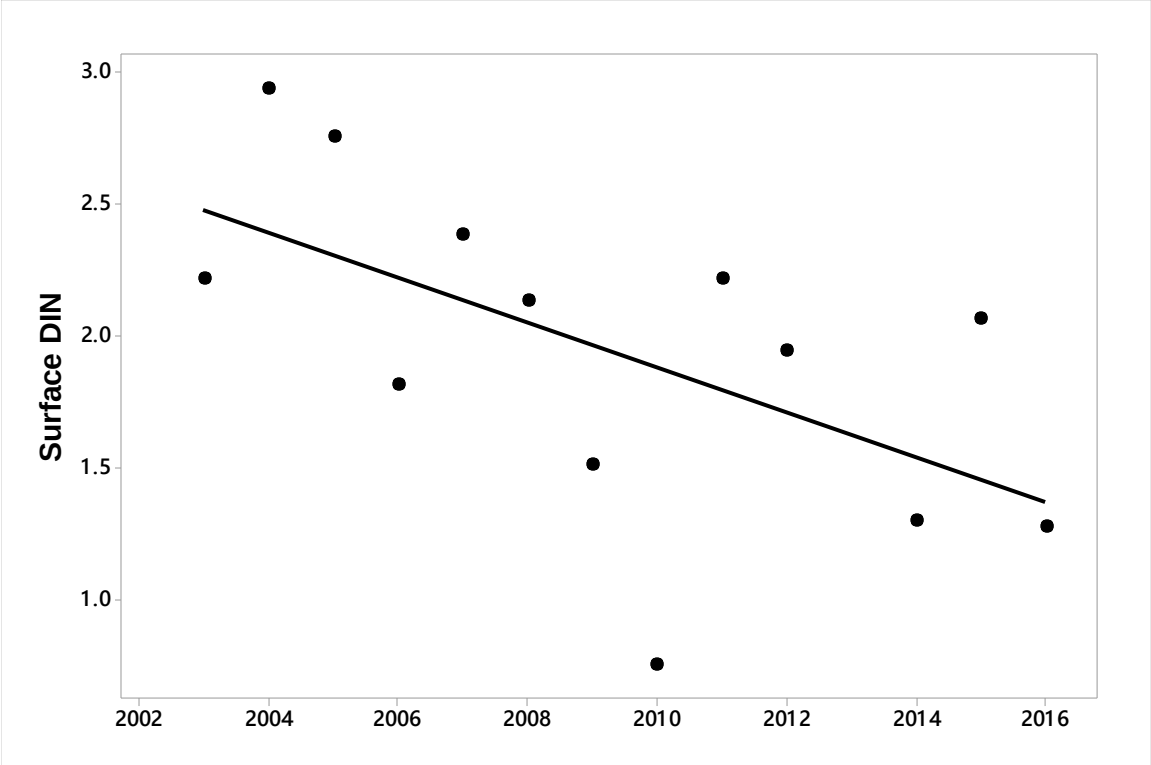

Figure R13-8. Surface dissolved inorganic nitrogen (DIN, µM) in the middle south domain vs. year with an R squared value of 35% and P < 0.05.

5. Phytoplankton

5.1. Phytoplankton Biomass and Size Structure during Late Summer to Early Fall in the Eastern Bering Sea

Contributed by: Lisa Eisner, Kristin Cieciel, Jeanette Gann, and Carol Ladd
NOAA - Alaska Fisheries Science Center
7600 Sand Point Way
Seattle, WA 98115

Methods: Variations in chlorophyll a (chl *a*) were used to evaluate spatial and interannual differences in total phytoplankton biomass and size structure. Phytoplankton dynamics determine the amount and quality of food available to zooplankton and higher trophic levels, and are thus important to ecosystem function. For example, larger phytoplankton assemblages may lead to shorter food webs and a more efficient transfer of energy to sea birds, fish and marine mammals.

The ratio of large phytoplankton biomass to total biomass (>10 µm chl *a*/ total chl *a* (GFF)) of water samples at discrete depth was estimated with standard fluorometric methods (Parsons et al., 1984). Integrated chl *a* values were estimated from CTD fluorescence profiles, calibrated with total chl *a* values at discrete depths. Chl *a* data were integrated (summed) over the top 50 m of the water column. Water column stability was estimated over the top 70 m (Simpson et al., 1978). Similarly, a stratification index was estimated

at Mooring 2 (M2) (Ladd and Stabeno, 2012; Eisner et al., 2015). Friction velocity cubed (u*3), a proxy for wind mixing, was obtained from NCEP reanalysis at M2 (courtesy of N. Bond).

Spatial distribution: Phytoplankton biomass were observed high over the southern outer shelf (between the 100-200 m isobaths) with highest values inshore of Bering Canyon, near the Pribilof Islands, and north of St. Lawrence Island (Figure R13-9A). Larger phytoplankton were observed on the inner shelf and near the Pribilof Islands, and smaller phytoplankton on the south middle and outer shelf (Figure R13-9B).

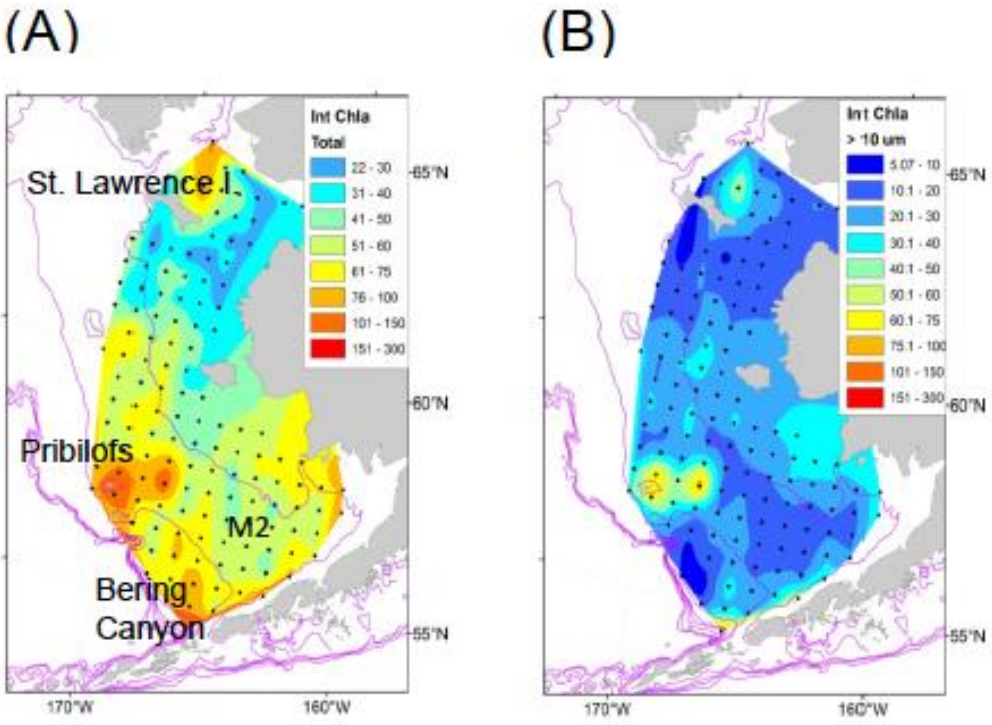

Figure R13-9. Contours of 0-50 m integrated total chl *a* (mg m^2) (A) and >10 µm chl *a* (B) averaged over 2003-2012.

Trend:
Integrated chl a: Total chl *a* and the mean size of phytoplankton assemblages was higher in early warm (2003-2005) than in cold (2006-2012) years in the south (Table R13-1). In contrast, in later warm years (2014-2016) total chl *a* was average, whereas large size fraction were below average especially in 2014 both in south and north, which had the lowest percent large (highest % small) phytoplankton for the time series (Figure R13-10). This 2014 anomaly was due to an extensive coccolithophore bloom over the north and south middle shelf.

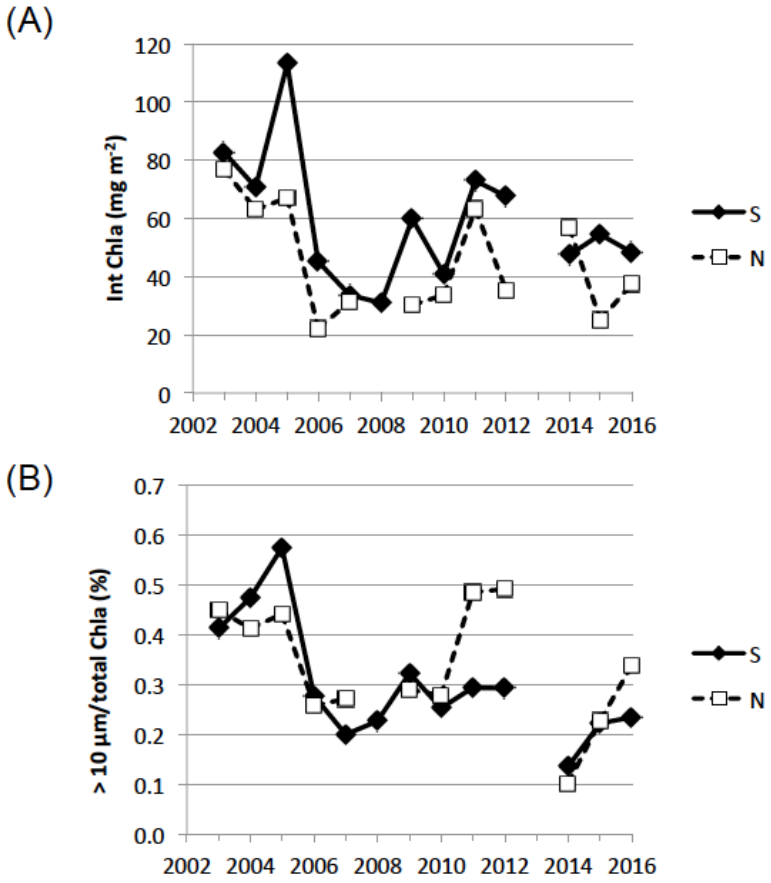

Figure R13-10. 0-50 m time-series of Integrated total chl *a* (A) and ratio of large phytoplankton assemblages to total (>10 µm/total chl *a*) (B) in the middle shelf in the south and north for 2003-2016. No survey in 2013.

Wind mixing: For the southern middle shelf, a positive association was observed between August u*3 (wind mixing 2-3 weeks prior to chl *a* sampling) and integrated chl *a* over the top 50 m (Figure R13-11). Deep nutrient-rich waters may be mixed to the surface to fuel production of large assemblages during periods of high winds and low water column stability.

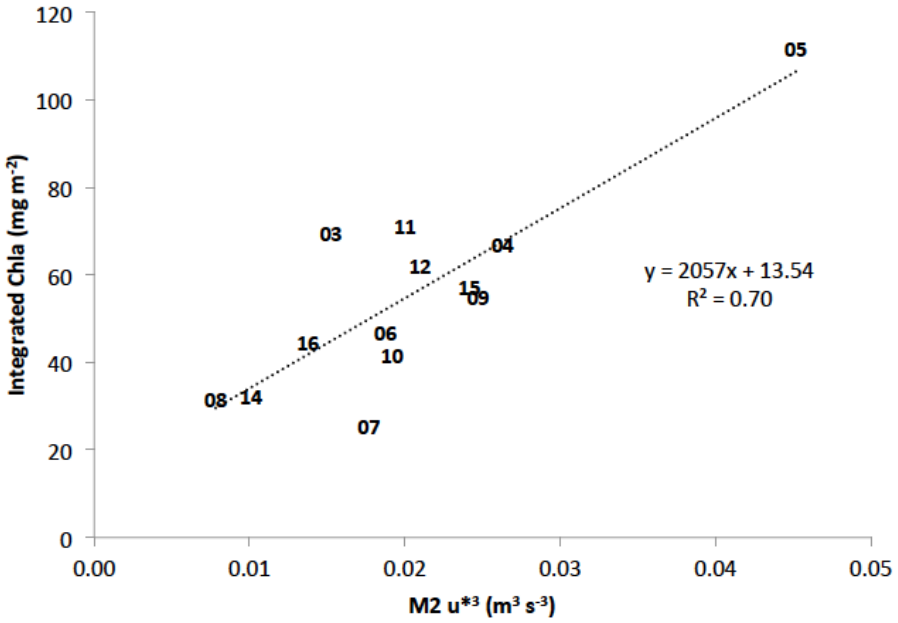

Figure R13-11. Linear regression between mean August u*3, an indicator of wind mixing, at Mooring M2 and integrated chl *a* for the southeastern Bering Sea middle shelf for 2003-2016 (no 2013 data).

Temperature: Phytoplankton growth may be enhanced at higher temperatures, depending on species. For example, the lowest chl *a* and smallest size fractions were observed in 2008, a period with low wind mixing, high stability and low water column temperature (Table R13-1).

Table R13-1.
Normalized anomalies (mean yearly value minus average value normalized by standard deviation) for 2003 to 2016 (or to 2012 for stratification index) for the south middle shelf. Anomalies were calculated for temperature (T) above and below the pycnocline, friction velocity cubed (u*3) at Mooring M2, August stratification index, integrated chl *a*, and ratio of large (>10 µm) to total chl *a*. Year is colored as red for warm, black for average, and blue for cold. Shading indicates if anomaly is positive (dark gray, >0.5), small (no shading, -0.5 to 0.5) or negative (light gray, <-0.5).

	2003	2004	2005	2006	2007	2008	2009	2010	2011	2012	2013	2014	2015	2016
T above	**0.7**	**1.1**	**0.4**	**-0.1**	**-0.2**	**-0.8**	**-1.3**	**-0.9**	**-0.9**	**-1.2**	NA	**1.5**	**0.3**	**1.6**
T below	**0.4**	**0.3**	**0.6**	**-0.2**	**-0.3**	**-0.4**	**-0.3**	**-0.6**	**-0.1**	**-0.6**	NA	**0.1**	**0.3**	**0.7**
u*^{3}	**-0.5**	**0.6**	**2.7**	**-0.2**	**-0.3**	**-1.3**	**0.5**	**-0.1**	**0.0**	**0.1**	NA	**-1.1**	**0.4**	**-0.7**
Stratification Index	**0.3**	**1.6**	**0.6**	**-0.6**	**1.5**	**-1.1**	**-0.8**	**-0.1**	**0.0**	**-1.3**				
Int chla	**1.0**	**0.5**	**2.4**	**-0.6**	**-1.1**	**-1.2**	**0.0**	**-0.8**	**0.6**	**0.4**	NA	**-0.5**	**-0.2**	**-0.5**
Large chla ratio	**0.9**	**1.4**	**2.3**	**-0.2**	**-0.8**	**-0.6**	**0.2**	**-0.4**	**-0.1**	**-0.1**	NA	**-1.4**	**-0.6**	**-0.6**

5.2. Coccolithophores in the Bering Sea

Contributed by: Carol Ladd[1], Sigrid Salo[1], and Lisa Eisner[2]
[1]NOAA/PMEL, Building 3, 7600 Sand Point Way NE, Seattle, WA 98115-6349
[2]NOAA/Alaska Fisheries Science Center

Methods: Blooms of coccolithophores are easily observed by satellite ocean color instruments due to their high reflectivity. Using methodology developed by Iida et al. (2002, 2012), we identify the number of satellite ocean color pixels associated with coccolithophores. Because blooms are often largely confined to either the middle shelf or the inner shelf, two indices are calculated, one for the inner shelf (30-50m depth) and one for the middle shelf (50-100 m depth. Using only days that are more than 50% cloud-free, coccolithophore indices were calculated as an average area (km^2) covered by coccolithophore blooms during the month of September of each year.

Variability in the dominant phytoplankton (diatoms vs. coccolithophores) is likely to influence trophic connections with the smaller coccolithophores resulting in longer trophic chains. Coccolithophores may be a less desirable food source for microzooplankton in this region (Olson and Strom, 2002) and the striking milky aquamarine color of the water can also reduce foraging success for visual predators.

Trends: Annual images (Figure R13-12) show the spatial and temporal variability of coccolithophore blooms in September. Coccolithophore abundance was particularly high during the early part of the record (1997-2000), with an index (averaged over the 3 years) of 120,075 km^2 for the middle and inner shelf combined (Figure R13-13). In 2001, the index dropped to 21,044 km^2 and remained low (<50,000 km^2) through 2006. In 2007, the index rose above 75,000 km^2. A higher index (> 50,000 km^2) was observed in 2007, 2009, 2011, 2014, and 2016 for the middle shelf and in 2011 and 2014 (> 20,000 km^2) for the inner shelf. September 2017 exhibited the lowest index of the record with 9 km^2 over the middle shelf and 431 km^2 over the inner shelf for a total of 440 km^2.

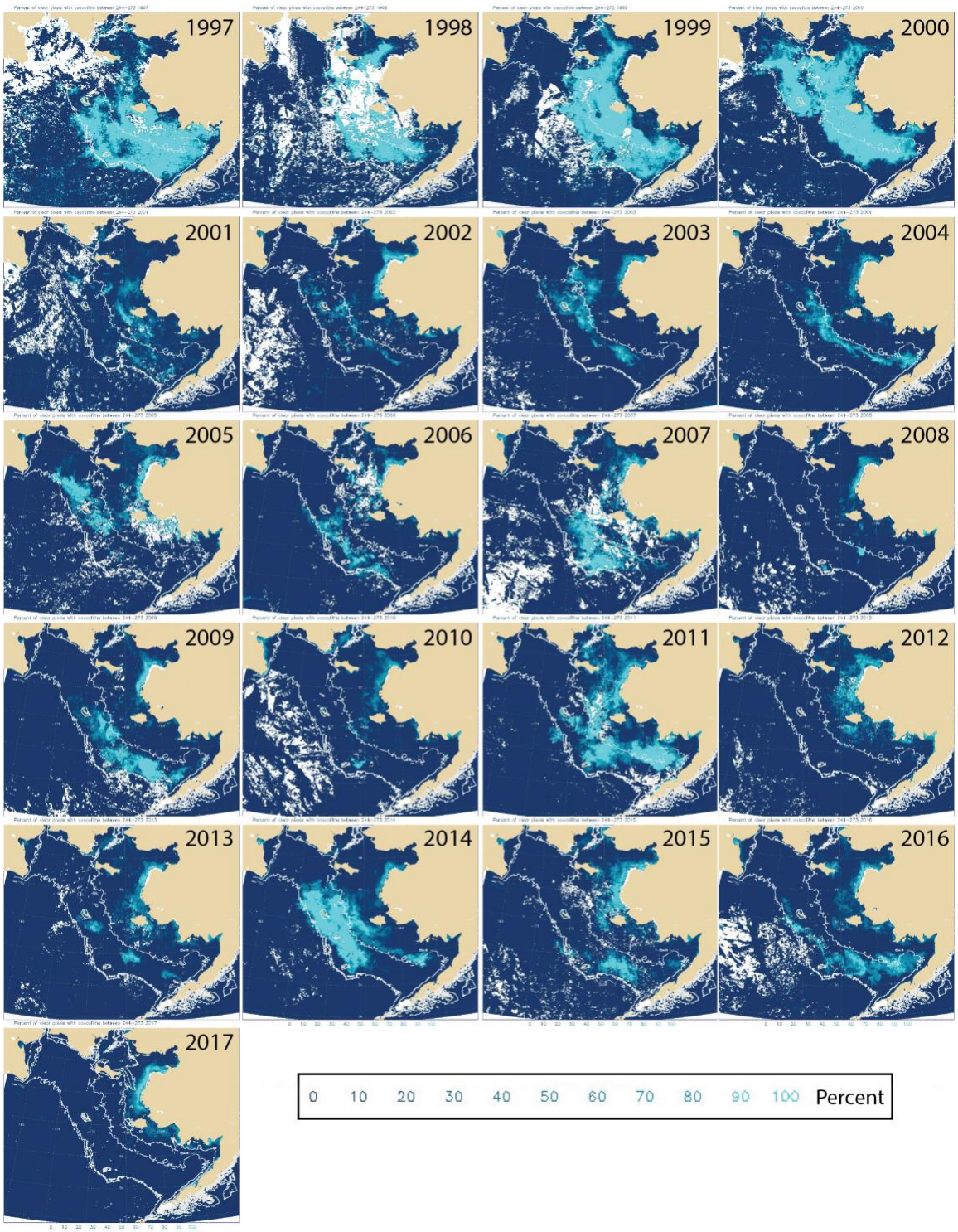

Figure R13-12: Maps illustrating the location and extent of coccolithophore blooms in September of each year. Color indicates the percent of cloud-free days in September for which each satellite ocean color pixel indicates coccolithophores.

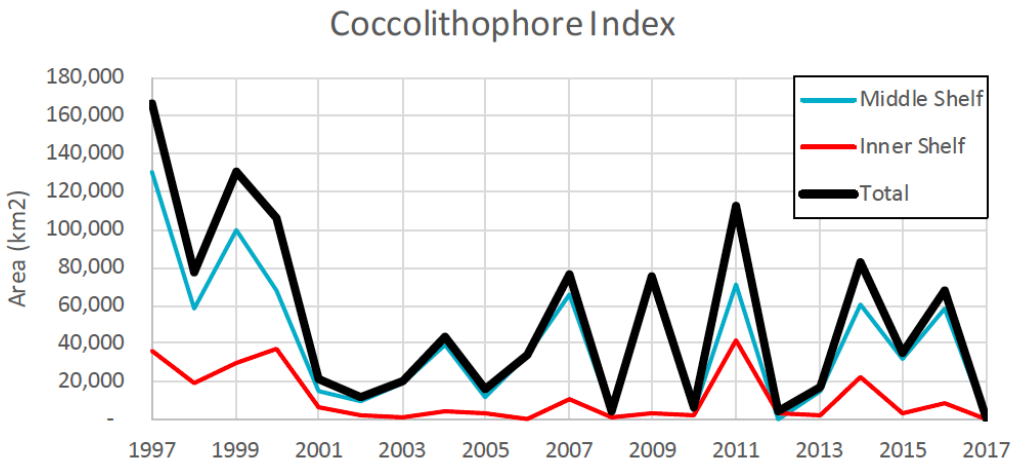

Figure R13-13. Coccolithophore index for the southeastern Bering Sea shelf (south of 60ºN). Red: average over the inner shelf (30-50 m depth); Blue: average over the middle shelf (50-100 m depth): Black: Total.

6. Zooplankton

6.1. Continuous Plankton Recorder

Contributed by: Sonia Batten
Sir Alister Hardy Foundation for Ocean Sciences
c/o 4737 Vista View Cr, Nanaimo BC, V9V 1N8, Canada

Methods: The Continuous Plankton Recorder (CPR) is towed behind a commercial ship at a depth of about 7 m. The plankton are collected continuously but then sectioned into 18.5 km samples (10 nautical miles), and every 4th sample is processed (see the sampling location in Figure R13-14) Position, date, and time information of the sample is taken from ship's log information and refers to the midpoint of the 18.5 km sample. Sampling began in 2000 and data are complete up to October 2016. Sampling is usually 3 times per year in this region, in spring, summer and autumn; however, owing to storms the ship did not sample this region in much of 2015 and 2016. Phytoplankton data are semi-quantitative and only a part of the community is sampled as not all cells are preserved by formalin, and many are too small to be retained by the 270 µm mesh or recorded under a light microscope. Taxonomic resolution of zooplankton varies, most copepods are identified to species and sometimes to stage. Gelatinous plankton are not well sampled and identified to only a coarse level of resolution. Further information on CPR analysis can be found in Batten et al (2003).

Trends (Figure R13-15): There is no trend in diatoms; 2008, 2010-12 were average, while numbers were higher in 2009, 2013-14. Mesozooplankton was high in 2008, then declined through 2012 before increasing in 2013 and 2014. Copepod size shows no trend, showing only modest variability over the time series.

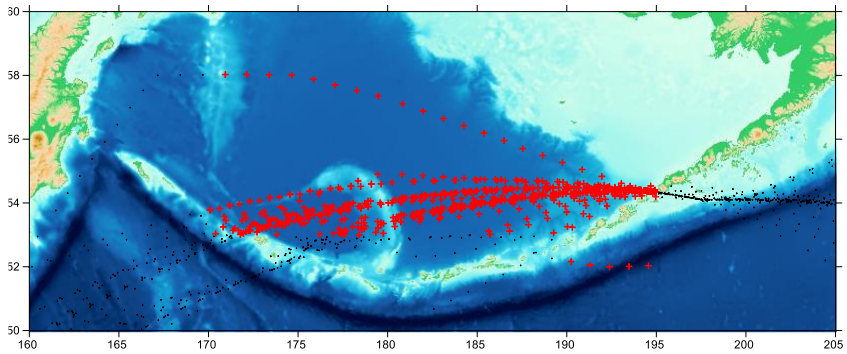

Figure R13-14. Location of CPR samples in Region 13, shown in red.

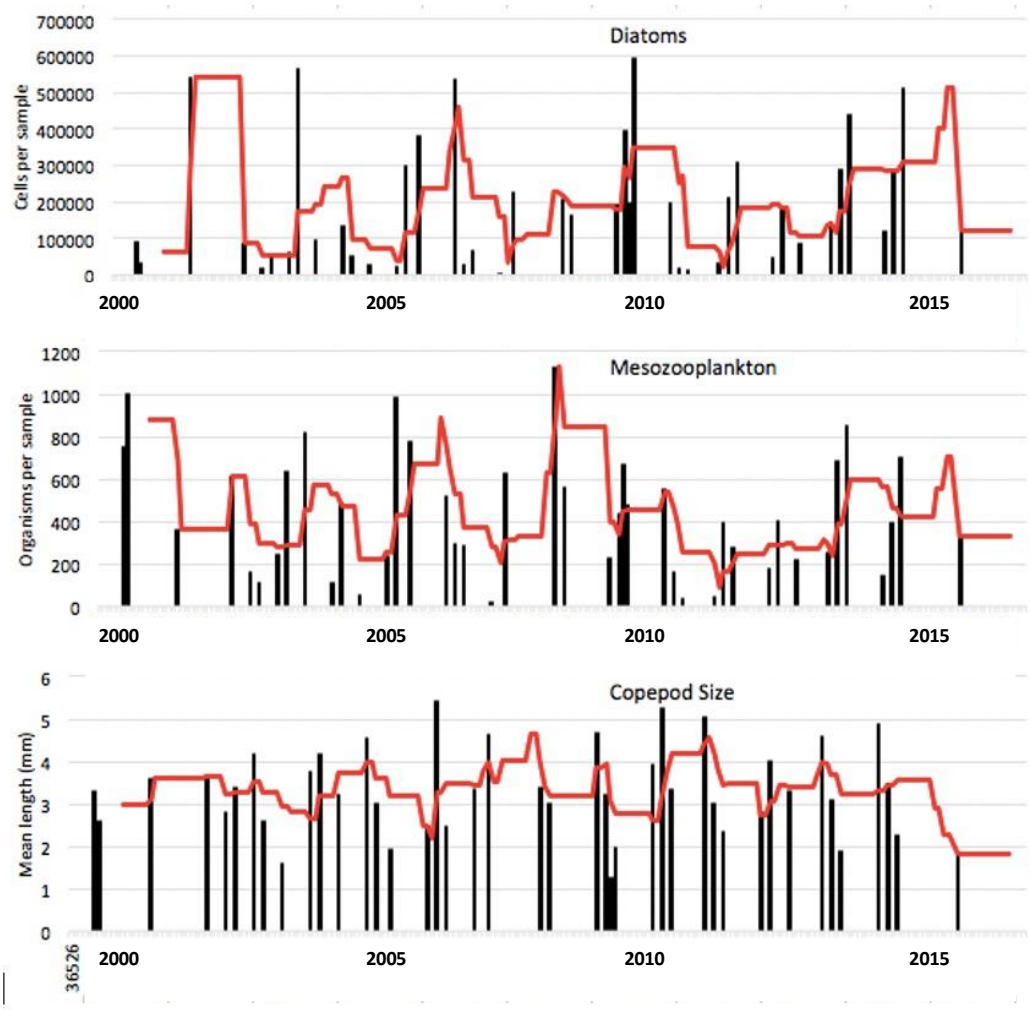

Figure 13-15. Time-series of phytoplankton and zooplankton variables obtained by CPR survey. Top: total diatom abundance (combined abundance of all diatom taxa per sample); Middle: mesozooplankton abundance (combined abundance of all zooplankton taxa per sample, with the exception of ciliates and eggs of copepods/euphausiids/fish); Bottom: the time series “Copepod Size” (mean length of copepods caught, assuming a standard length per taxon equal to the length of an adult female). Data for all samples collected in the region per month were averaged to give a monthly mean, presented as black bars. The red line indicates a 12-month running mean to show the long term trends.

6.2. Eastern Bering Sea Euphausiids (Krill)

Contributed by Patrick Ressler
NOAA - Alaska Fisheries Science Center

Methods: Acoustic backscatter classified as euphausiids was used to compute the numerical density (no./ m^3) of euphausiids in 0.5 nm intervals along acoustic-trawl survey transects on the middle and outer eastern Bering Sea continental shelf between approximately 54 – 62° N and 158 – 180° W. These values were then averaged over the water column and across the surveyed area to produce annual averages. Because few trawl samples were available in the early years of the times series, the parameter used to convert euphausiid backscatter to numerical density (target strength; Smith et al. (2013)) was modeled using the average of length and species composition from samples collected 2004-2016 (2018 sample counts not yet available). Error bars on annual values indicate 95% confidence intervals computed from geostatistical estimates of relative estimation error due to sampling variability (Petitgas, 1993).

Trends: *Thysanoessa inermis* dominated species composition on the outer shelf and *T. raschii* dominated inshore. There is some indication that euphausiids were smaller in 2004-2009 and in 2016 (by 1-2 mm), and that there was an increase in relative abundance of *T. spinifera* in 2016, compared to other years. Summertime euphausiid density increased from 2004-2009, then subsequently declined 2010 through 2016, when the lowest value in the time series was reported (Figure R13-16). Euphausiid density increased slightly in summer 2018 from 2016, but remains relatively low. The 2018 value is similar to what was observed in 2004, a year with very low euphausiid densities according to data from many sources (reviewed in Hunt et al. 2016).

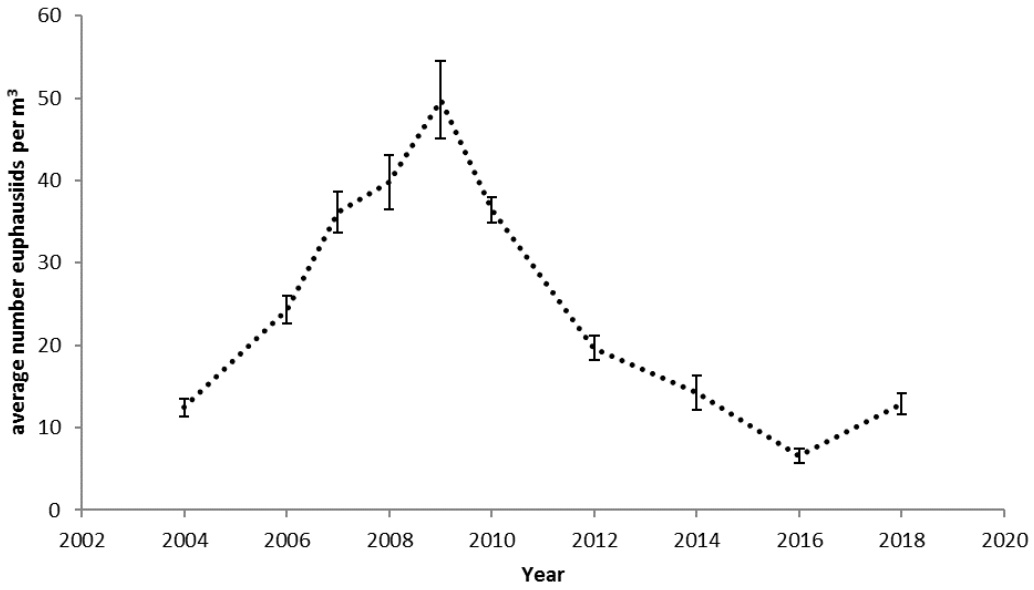

Figure R13-16. Acoustic estimate of average euphausiid abundance (no./ m^3). Error bars are approximate 95% confidence intervals computed from geostatistical estimates of sampling error (Petitgas, 1993).

6.3. Rapid Zooplankton Assessment and Historical Time Series for the Eastern Bering Sea

Contributed by David Kimmel[1], Jesse Lamb[1], Nissa Ferm[1], Corey Fugate[2], and Colleen Harpold[1]
[1]Resource Assessment and Conservation Engineering Division
[2]Auke Bay Laboratories

Methods: The Rapid Zooplankton Assessment (RZA) provides preliminary estimates of zooplankton abundance and community structure. The method employed uses coarse categories and standard zooplankton sorting methods (Harris et al., 2005). The categories are small copepods (<2 mm; example species: *Acartia* spp., *Pseudocalanus* spp., and *Oithona* spp.), large copepods (>2 mm; example species: *Calanus* spp. and *Neocalanus* spp.), and euphausiids (<15 mm; example species: *Thysanoessa* spp.). Small copepods were counted from the 153 µm mesh, 20 cm bongo net. Large copepods and euphausiids
were counted from the 505 µm mesh, 60 cm bongo net. In 2016, the method was refined and personnel counted a minimum of 100 organisms per sample at sea to improve zooplankton estimates. Other rarer zooplankton taxa were present but were not sampled effectively with the on-board sampling method. Detailed information on these taxa is provided after in-lab processing protocols have been followed (1+ years post survey).

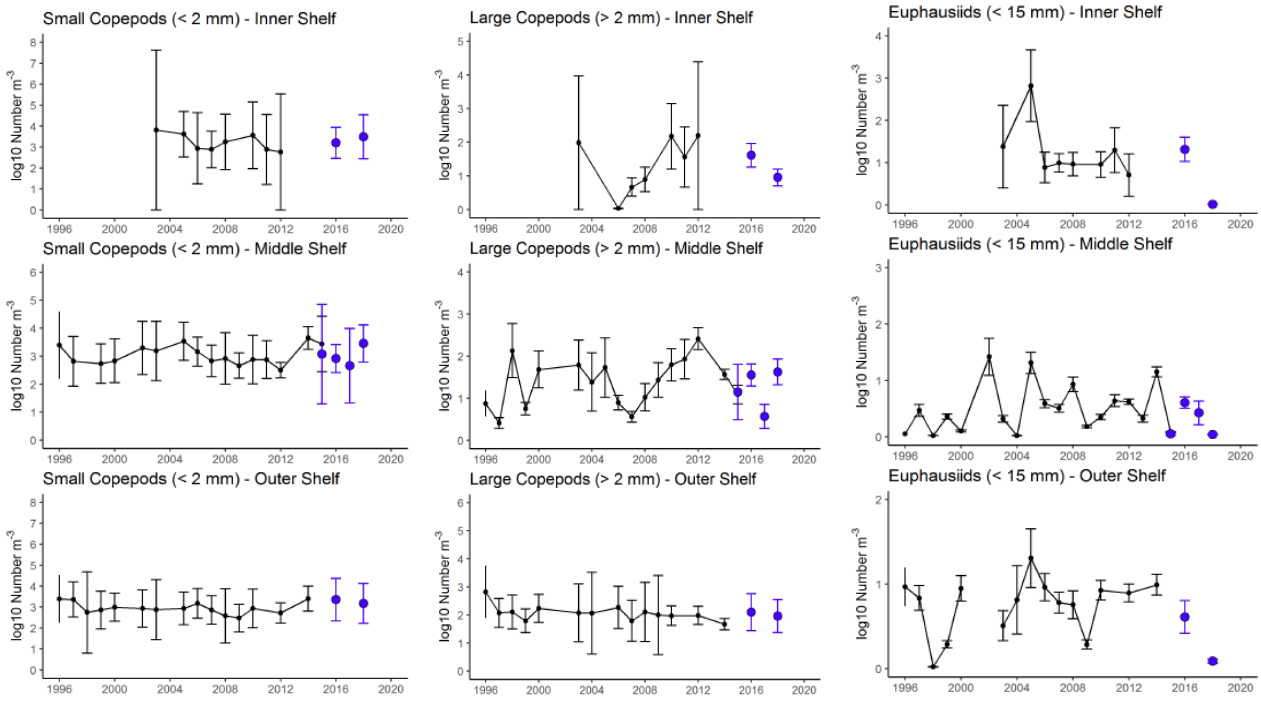

Figure R13-17 Annual mean abundances of small (<2 mm) copepods (left), large (>2 mm) copepods (middle), and euphausiids (<15 mm) (right) in the southeastern Bering Sea. Black points and lines represent FOCI archived data, blue points represent RZA data. Error bars represent standard error of the mean. Note differences in scale.

To provide comparison to yearly RZA data, long-term time-series for the inner, middle, and outer domains were developed from archived data. The mean spring abundance of each RZA category was plotted for the southern inner, middle, and outer shelf of the Bering Sea (Ortiz et al., 2012) and represented primarily April and May as the months with the greatest sampling frequency. Plotted on the time-series were the RZA estimates from the corresponding location and year, presented as an annual mean.

Trends (Figure R13-17): Small copepod abundances have shown little variability in all areas since 2009. More recent (2018-2019) small copepod abundances have matched previous high values of 2014-2015. The increase in spring temperatures seen in recent years has resulted in the increased small copepod abundances observed. This is because small copepod growth rates and development times are strongly related to temperature. Large copepod abundances, primarily *Calanus marshallae/glacialis*, increased along the inner and middle shelves from 2009-2012 during the prolonged cold stanza. More recently (2017-2019) large copepod abundances were lower than the cold period and fluctuated annually along the inner and middle shelves. Large copepods more common on the outer shelf (e.g., *Neocalanus* spp.) did not follow this pattern. Euphausiid abundances show considerable variability over time regardless of location and more recent (2018-2019) abundances have been low across the Bering Sea shelf.

6.4. Jellyfishes on the Eastern Bering Sea Shelf

Contributed by Robert Lauth and Elizabeth Dawson
Resource Assessment and Conservation Engineering Division, Alaska Fisheries Science Center, National Marine Fisheries Service, NOAA

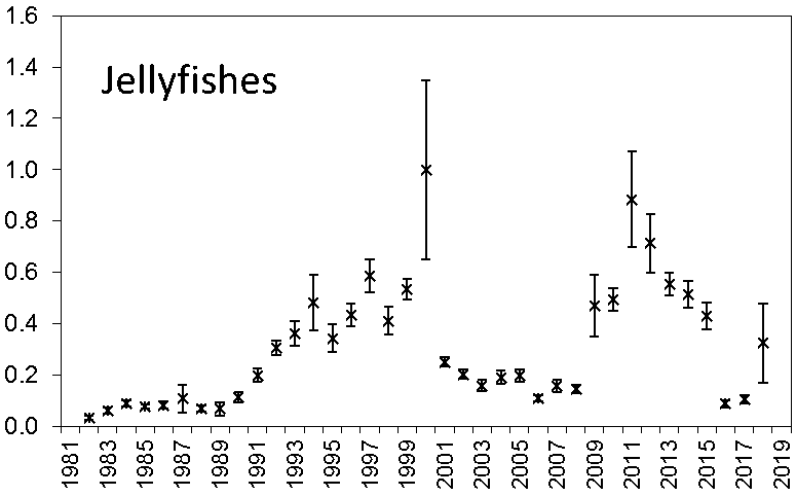

Figure R13-18. Relative Catch-Per-Unit-Effort (CPUE) for jellyfish during the May to August time period from 1982-2018. Data were obtained by Eastern Bering Sea shelf bottom trawl survey.

Methods: Relative Catch-Per-Unit-Effort (CPUE) was calculated by setting the largest biomass in the time series to a value of 1 and scaling other annual values proportionally. The standard error (±1) was weighted proportionally to the CPUE to produce a relative standard error. Jellyfish are pelagic consumers of zooplankton, larval and juvenile fishes,

and small forage fishes. A large influx of pelagic consumers such as jellyfish can decrease zooplankton and small fish abundance, which in turn can affect higher trophic levels causing changes to the community structure of the ecosystem.

Trends (Figure R13-18): There was a period of increasing biomass of jellyfishes throughout the 1990's (Brodeur et al., 1999) followed by a period of relatively low CPUE from 2001-2008 and then a second period with relatively higher CPUE values from 2009-2015. The relative CPUE for jellyfishes in 2018 increased by 211% from 2017, returning the 2018 estimate within a similar catch range as observed in the mid 1990's and in 2009 and 2010. The low CPUE values observed during 2016 and 2017 were within the range of those observed during the first nine years of the time series (1982-1991).

6.5. Trends in the Abundance of Jellyfish in the Eastern Bering Sea, 2004-2018

Contributed by: Kristin Cieciel, Ellen Yasumiishi, and Andrew Dimond
NOAA – Alaska Fisheries Science Center
17109 Pt. Lena Loop Rd., Juneau, AK 99801

Methods: Jellyfish were sampled using a trawl net towed in the upper 25m of the eastern Bering Sea during late summer, 2004-2018. Jellyfish catch was estimated in kilograms. Surveys were not conducted in the south (<60°N) during 2013 and 2015 and north (>60°N) during 2008. All jellyfish medusae caught in the surface trawl were sorted by species and subsampled for bell diameter and wet weight. Five species are commonly caught with the surface trawl: *Aequorea* sp., *Chrysaora melanaster* (hereafter '*Chrysaora*'), *Cyanea capillata*, *Aurelia labiata*, and *Staurophora mertensi*. Abundance was estimated for each species and region using the VAST package (version 1.5.0) for multispecies version 1.1.0 (Thorson et al., 2015; Thorson and Kristensen, 2016; Thorson et al., 2016a,b).

Trends (FigureR13-19): In 2018, jellyfish abundance was about 25% lower than 2016. Abundance was generally higher in the south than in the north, but trends in abundance were similar, except for the high abundances in 2014, due to *Chrysaora*. *Chrysaora* was the most abundant species until reaching a low level in 2018, when *Aequorea* dominate. 2014 was a peak abundance year for *Chrysaora*. *Aequorea* catches were high in 2016 and 2018. In the north, the relative abundance during 2018 compared to 2017 increased for *Aequorea*, *Cyanea*, and *Staurophora* and decreased for *Aurelia* and *Chrysaora*. In the south, the relative abundance was high and increased for *Aequorea* and *Aurelia*, and was low and declined for *Staurophora* and *Chrysaora* in 2018 relative to 2016. *Chrysaora* appears to be returning to lower levels similar to 2004-2007.

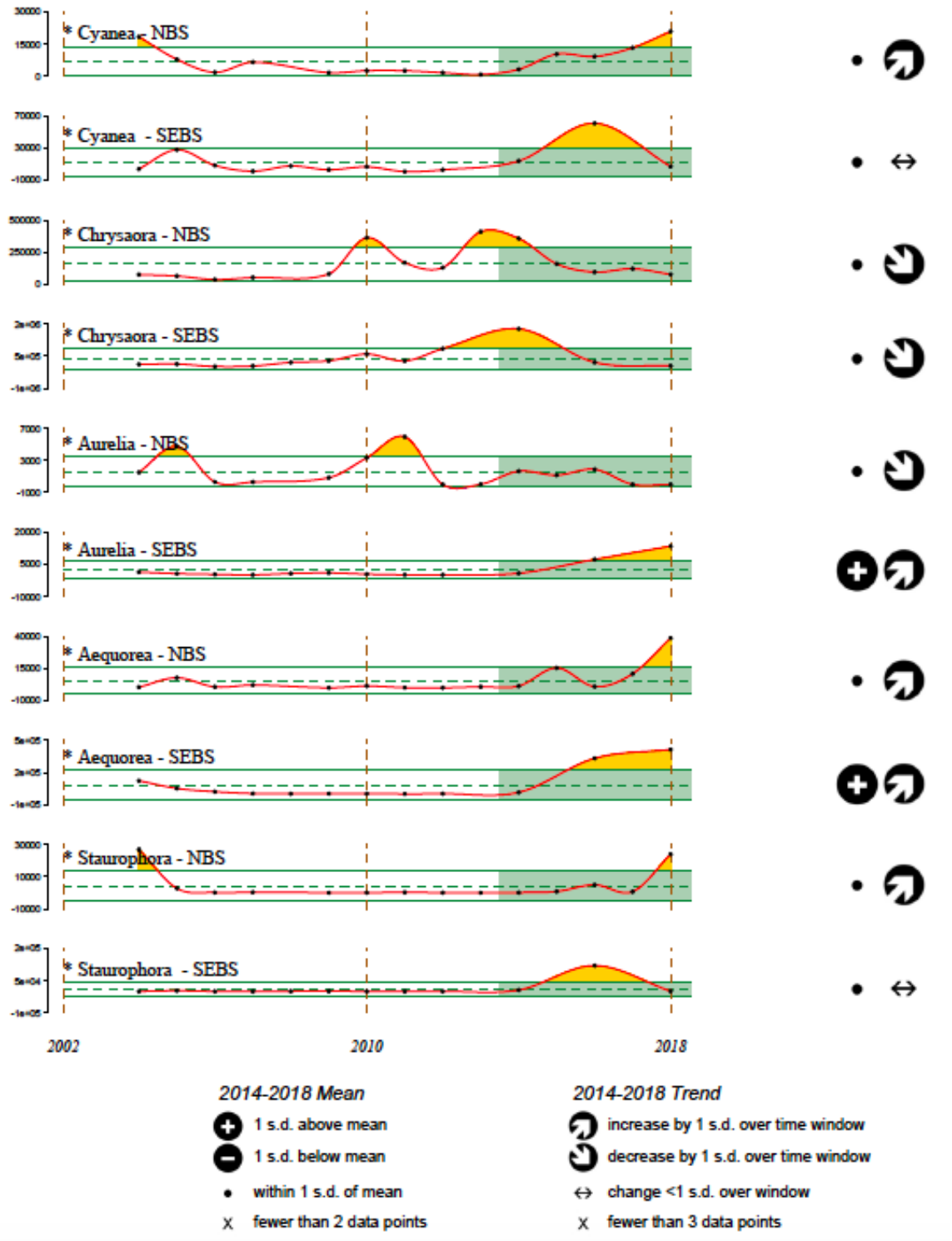

Figure R13-19. Time-series abundance (metric tonnes) of jellyfish in the eastern Bering Sea during late summer, 2004-2018. Broken and solid green line indicate mean and 1 standard deviation for 2004-2018, respectively.

7. Fishes and Invertebrates

7.1. Aggregated Catch-Per-Unit-Effort of Fish and Invertebrates in Bottom Trawl Surveys on the Eastern Bering Sea Shelf, 1982-2018

Contributed by Franz Mueter[1] and Robert Lauth[2]
[1]University of Alaska Fairbanks, 17101 Point Lena Loop Road, Juneau, AK 99801
[2]Resource Ecology and Fisheries Management Division, Alaska Fisheries Science Center, National Marine Fisheries Service, NOAA

Methods: The Catch-Per-Unit-Effort (CPUE) index provides a measure of the overall biomass of demersal and epibenthic fish and invertebrate species. We CPUE (in kg ha^{-1}) of fish and major invertebrate taxa for each successful haul completed during standardized bottom trawl surveys on the eastern Bering Sea shelf (EBS), 1982-2018. Total CPUE for each haul was computed as the sum of the CPUEs of all taxa. To obtain an index of average CPUE by year across the survey region, we modeled log-transformed total CPUE (N = 13,714 hauls) as a smooth function of depth, Julian Day, and location (latitude/longitude) with year-specific intercepts using Generalized Additive Models. Hauls were weighted based on the area represented by each station. The CPUE index does not account for gear or vessel differences, which are confounded with interannual differences and may affect results prior to 1988.

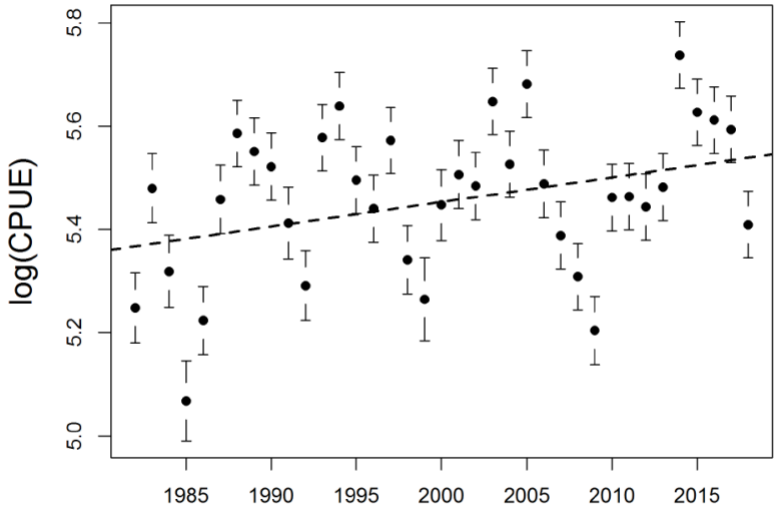

Figure R13-20. Model-based estimates of total log(CPUE) for major fish and invertebrate taxa captured in bottom trawl surveys from 1982 to 2018 in the Bering Sea with approximate pointwise 95% confidence intervals and linear time trend. Estimates were adjusted for differences in depth, day of sampling, and sampling locations among years. Gear differences prior to 1988 were not accounted for. The linear time trend, based on generalized least squares regression assuming 1st order auto-correlated residuals, was not statistically significant at the 95% significance level (t=1.332, p=0.191).

Trends (Figure R13-20): Total log(CPUE) in the EBS shows 6-10 year fluctuations and an apparent, but not statistically significant, increase over the entire time series with the highest observed value occurring in 2014. Total CPUE declined after 2014 and dropped sharply between 2017 and 2018. Estimated means prior to 1988 may be biased due to

unknown gear effects and because annual differences are confounded with changes in mean sampling date, which varied from as early as June 15 in 1999 to as late as July 16 in 1985. On average, sampling occurred about a week earlier since the 2000s compared to the 1980s. Over the focal period from 2009 to 2016, total CPUE increased substantially with two highly significant step-increases between 2009 and 2010 and another increase between 2013 and 2014. The estimated median CPUE in 2015/16 (275 kg ha^{-1}) was 34% higher than in 2009 (181 kg ha^{-1}), which represented a 30-year low because of declines in walleye pollock (*Gadus chalcogrammus*) associated with a series of weak year-classes in 2001-2005.

7.2. Eastern Bering Sea Groundfish Condition

Contributed by: Jennifer Boldt, Chris Rooper, and Jerry Hoff
NOAA - Alaska Fisheries Science Center

Methods: Fish condition may affect fish growth and subsequent survival (Paul et al., 1998; Boldt and Haldorson, 2004) and may be an indicator of ecosystem productivity. Length-weight residuals are an indicator of somatic growth relative to the mean (Brodeur et al., 2004) and, therefore, a measure of fish condition that estimates how heavy a fish is per unit body length. Positive length-weight residuals indicate fish are in better condition (i.e., heavier per unit length); whereas, negative residuals indicate fish are in poorer condition (i.e., lighter per unit length).

Individual lengths and weights collected during the summertime NOAA Alaska Fisheries Science Center eastern Bering Sea shelf bottom trawl survey for pollock, Pacific cod, Arrowtooth flounder, Yellowfin sole, Flathead sole (*Hippoglossoides elassodon*), Northern rock sole (*Lepidopsetta polyxystra*), and Alaska plaice (*Pleuronectes quadrituberculatus*) were used in this analysis of fish condition. Length-weight relationships for each of the seven species were estimated with a linear regression of log-transformed values overall years where data was available (during 1982-2018). Additionally, length-weight relationships for age 1+ pollock (length from 100-250 mm) were also calculated independent from the adult life history stages. Residuals from the length-weight relationships were averaged for the entire eastern Bering Sea. Temporal and spatial patterns in residuals were examined.

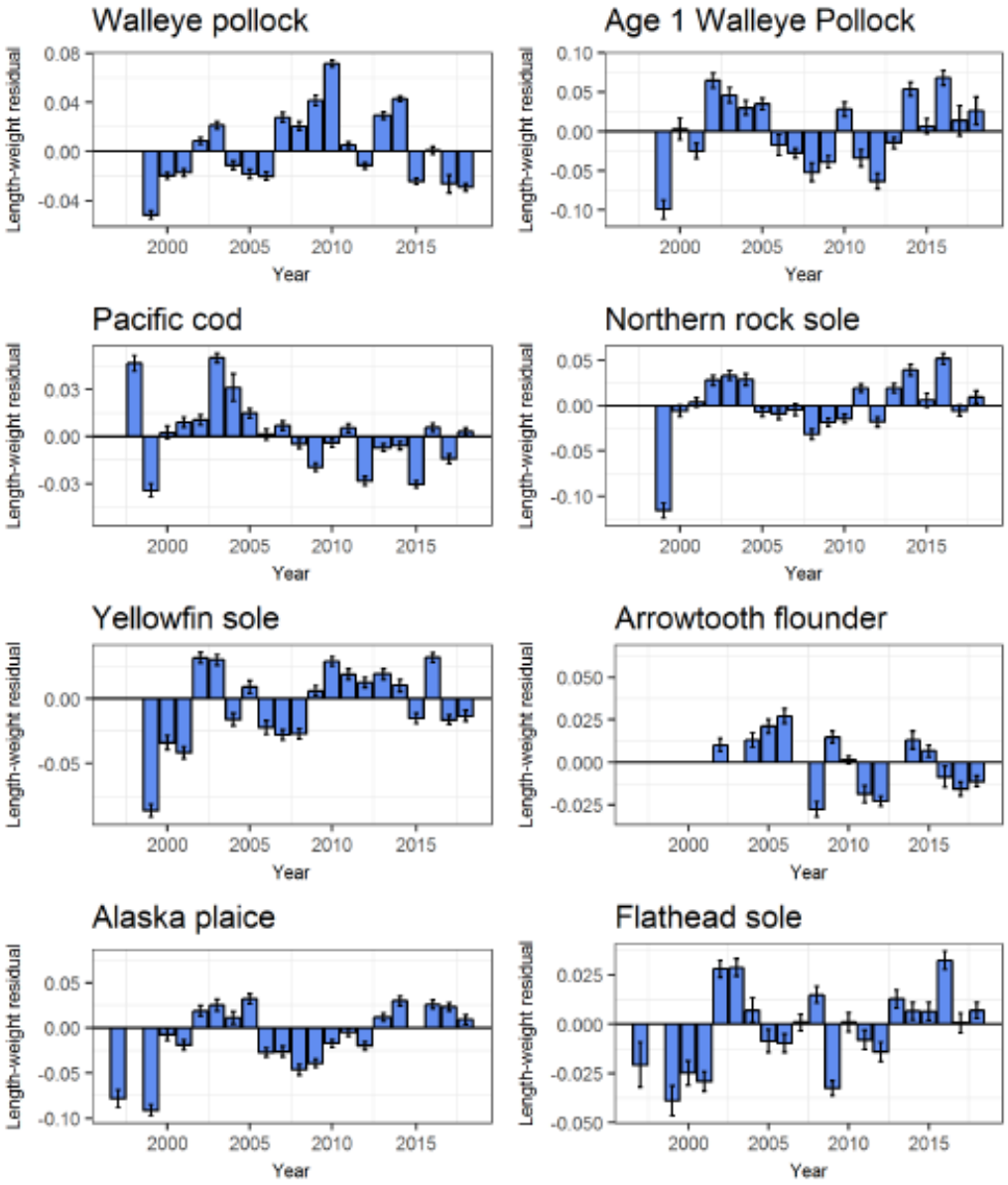

Figure R13-21. Length-weight residuals for seven eastern Bering Sea groundfish sampled in the NOAA Alaska Fisheries Science Center standard summer bottom trawl survey, 1997-2018.

Trends (Figure R13-21): Length-weight residuals have varied over time for all species with a few notable patterns . Residuals for all species where there was data were negative in 1999, a cold year in the Bering Sea. Residuals became positive or more positive in 2002 for five of the seven species examined. Flatfish residuals were generally positive from 2002 to 2004 or 2005 depending on species. Age-1 pollock and Pacific cod residuals were positive from 2001 to 2004 or 2005. In 2008, all species except Flathead sole and pollock had negative residuals. From 2009 to 2016 the condition of adult pollock and Pacific cod decreased, while age 1 pollock condition generally increased. For flatfish 2009-2016 was a period of increasing condition for Northern rock sole,

Flathead sole and Alaska plaice, while Yellowfin sole and Arrowtooth flounder condition showed a declining trend and no trend respectively.

7.3. Trends in Pelagic Forager Biomass in the eastern Bering Sea, 1982-2018

Contributed by: Stephani Zador
NOAA - Alaska Fisheries Science Center
7600 Sand Point Way NE, Seattle, WA 98115

Methods: This information represents the total biomass of fish in the pelagic foraging guild in the eastern Bering Sea shelf ecosystem. The pelagic foraging guild includes adult and juvenile pollock, other forage fish such as Pacific herring (*Clupea pallasii*), Capelin (*Mallotus villosus*), Eulachon (*Thaleichthys pacificus*), and Sandlance (*Ammodytes* spp.), pelagic rockfish (*Sebastes* spp.), salmonids (*Oncorhynchus* spp.), and squid. Information quality ranges from a sophisticated, highly quantitative stock assessment for pollock (the dominant biomass in the guild), to relatively high variance eastern Bering Sea shelf bottom trawl survey data for forage fish, and to no time series data for salmon and squid.

Trends (Figure R13-22): Survey biomass of pelagic foragers decreased in 2016 below its 34-year mean after increasing steadily from 2009 to 2015. This was primarily driven by the increase in pollock from its historical low in the survey in 2009. Pollock has followed the warm/cold stanzas to some degree. Pollock biomass began to drop during the early 2000s warm period, increased during the cold period, and then dropped again in 2016.

The decrease in forager guild biomass was also a result of fluctuations in Capelin, which increased during the cold years between 2010 and 2014, then dropped back to pre-2010 levels in 2016. Interestingly, Capelin remained abundant in the first warm year of 2015. There appeared to be no cohesive salmon response to the state of the ecosystem. The 2015 harvests for Chinook salmon (*O. tshawytscha*) were low, and coho salmon (*O. kisutch*) harvests were considerably lower than in 2014 (largest in the last 20 years).

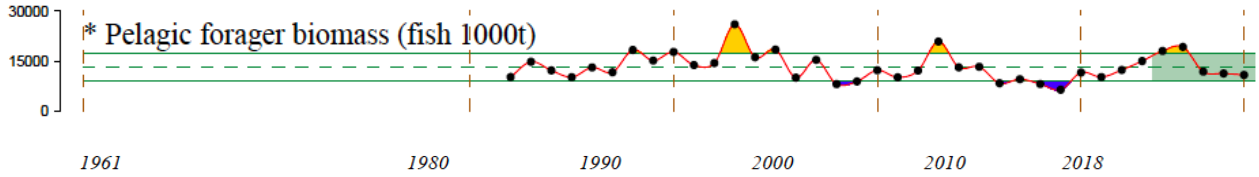

Figure R13-22. Biomass (metric tonnes) of pelagic foragers in NOAA trawl surveys in the eastern Bering Sea. Broken and solid green lines incidate overall mean and 1 x standard deviation.

7.4. Trends in of Forage Fish Abundance in the Eastern Bering Sea, 2002-2018.

Contributed by: Ellen Yasumiishi, Alex Andrews, Kristin Cieciel, Jim Murphy, Elizabeth Siddon, and Andrew Dimond
NOAA – Alaska Fisheries Science Center
17109 Pt. Lena Loop Rd, Juneau AK 99801

Methods: Fish were sampled using a trawl net towed in the upper 25m of the eastern Bering Sea during late summer, 2002-2018. Fish catch was weighed in kilograms at each station. Surveys were not conducted in the south (<60°N) during 2013, 2015, and 2017; and north (>60°N) during 2008 so no estimates of abundance were made for these years or regions. Eight species were commonly caught with the surface trawl: age-0 pollock, Capelin, Pacific herring, juvenile Chinook salmon, juvenile chum salmon (*O. keta*), juvenile pink salmon (*O. gorbuscha*), juvenile coho salmon, and juvenile sockeye salmon (*O. nerka*); for this analysis all non-Chinook salmon have been pooled into a juvenile salmon group. Biomass was calculated for each species or group and compared in the northern and southeastern regions of the Bering Sea. Few Chinook salmon were captured in the south so we did not estimate abuneances for these fish. Abundance was estimated for each species or group using the VAST package (version 1.5.0, cpp version) for multispecies version 1.1.0 (Thorson et al., 2015; Thorson and Kristensen, 2016; Thorson et al., 2016a,b).

Trends (Figure R13-23): Warm and cold year occurrences can be observed in the normalized time series of abundance of fish in pelagic waters. Capelin was typically more abundant during cold years, whereas herring was typically more abundant during warm years. Juvenile salmon abundances were higher during the recent warm stanza (2014-2018), but not during the earlier 2002-2005 warm stanza. Age-0 pollock also occurred in higher abundance during warm years than cold years.

In 2018, the abundance of pelagic fish species increased in the southeastern Bering Sea relative to 2016 and decreased in the northern Bering Sea relative to 2017. In the north, juvenile non-Chinook salmon (primarily pink and chum salmon) were the only fish group that was above average in 2018, while herring and capelin were below average and age-0 pollock was around the mean. In the south, the model-estimated abundance of juvenile salmon (primarily sockeye salmon) and herring were both above the overall average, while capelin was below the average and age-0 pollock was near the mean.

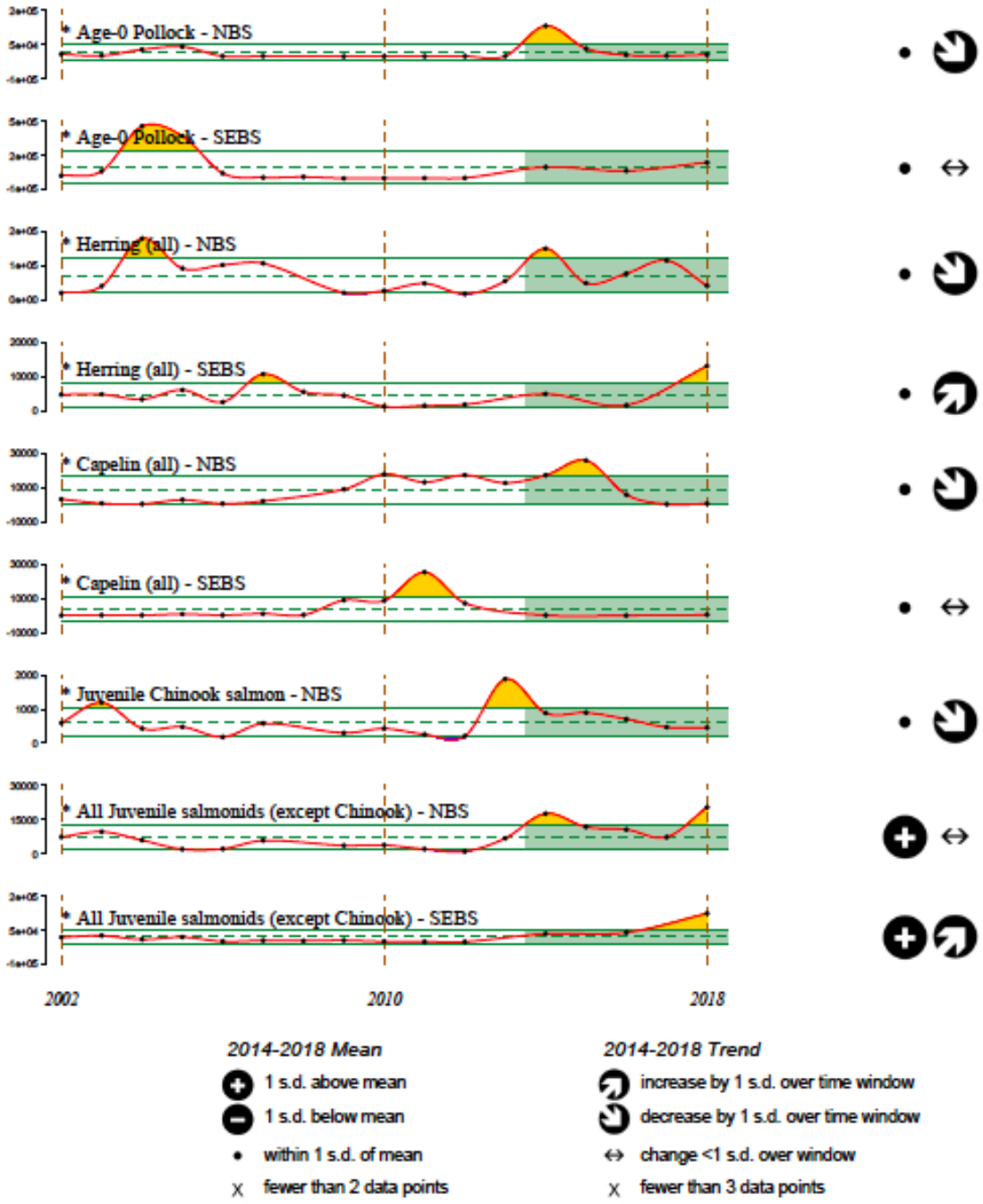

Figure R13-23. Relative abundance (metric tonnes) of forage fish in pelagic waters of the northern Bering Sea (NBS) and southeastern Bering Sea (SEBS) during late summer, 2002-2018. Broken and solid green lines indicate overall mean and 1 x standard deviation. Symbols on the right side indicate 2014-2018 trend and extent of the 2014-2018 mean relative to the 2002-2018 mean.

7.5. Trend in the Annual Inshore Run Size of Bristol Bay Sockeye Salmon (*Oncorhynchus nerka*)

Contributed by Curry J. Cunningham[1], Gregory Buck[2], Katie Sechrist[2], Jordan Head[2]
[1]Auke Bay Laboratories, Alaska Fisheries Science Center, National Marine Fisheries Service, NOAA
[2]Alaska Department of Fish and Game, Anchorage, Alaska

Methods: The annual abundance of adult sockeye salmon (*O. nerka*) returning to Bristol Bay, Alaska is enumerated by the Alaska Department of Fish and Game (ADF&G). The total inshore run in a given year is the sum of commercial catches in five terminal fishing districts plus the escapement of sockeye to nine major river systems. Total catch is estimated based on the mass of fishery offloads and the average weight of individual sockeye within time and area strata. Escapement is the number of fish successfully avoiding fishery capture and enumerated during upriver migration toward the spawning grounds, or through post-season aerial surveys of spawning grounds (Elison et al., 2012). Although there have been slight changes in the location and operation of escapement enumeration projects and methods over time, these data provide a consistent index of the inshore return abundance of sockeye salmon to Bristol Bay since 1963.

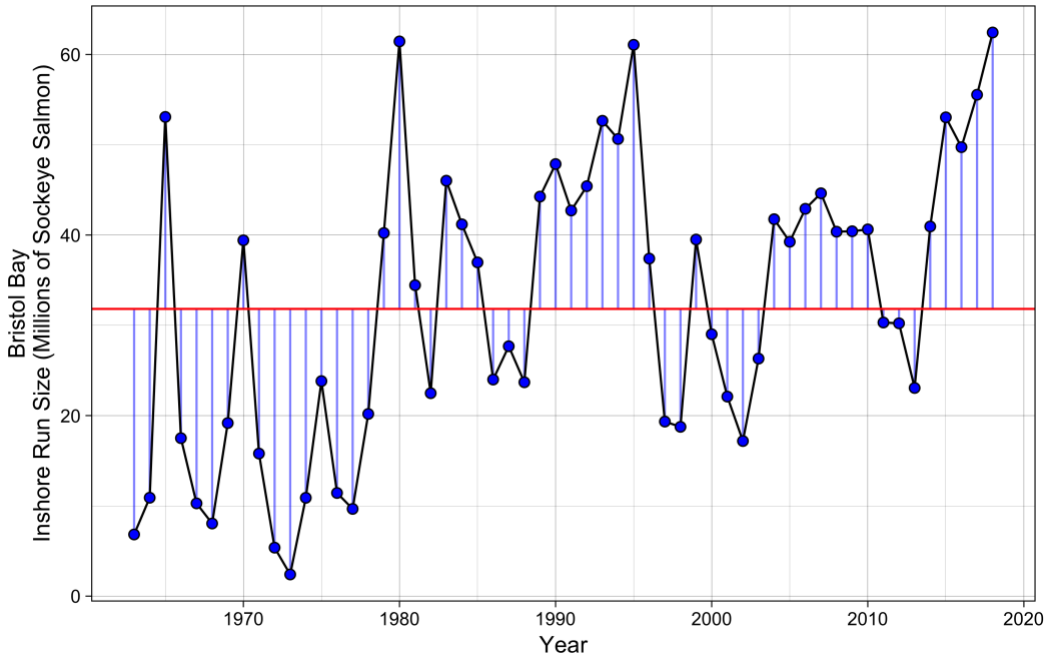

Figure R13-24. Annual Bristol Bay sockeye salmon inshore run size 1963-2018. Red line is the time series average of 32.4 million sockeye.

Trends (Figure R13-24 & 25): The 2018 Bristol Bay salmon inshore run of 63.0 million sockeye is the largest on record since 1963 and is 55.8% higher than the recent 10-year average of 40.4 million sockeye, and 98.0% higher than the 1963-2017 average of 31.8 million sockeye. The temporal trend in Bristol Bay sockeye salmon run size indicates a large increase during the recent 4-year period (2015-2018), with inshore run sizes above recent and long-term averages (Figure R13-24). The current period of high abundance is only paralleled by 1989-1995, during which inshore run sizes to the Naknek-Kvichak,

Egegik, and Ugashik commercial fishing districts were all above respective long-term averages (Figure R13-25). Also of note, inshore runs to the Nushagak District in 2018 and 2017 are the first and second highest on record since 1963, which at 33.5 and 20.0 million sockeye, were 395.4% and 196.1% higher than the 1963-2018 average of 6.8 million sockeye (Figure R13-25).

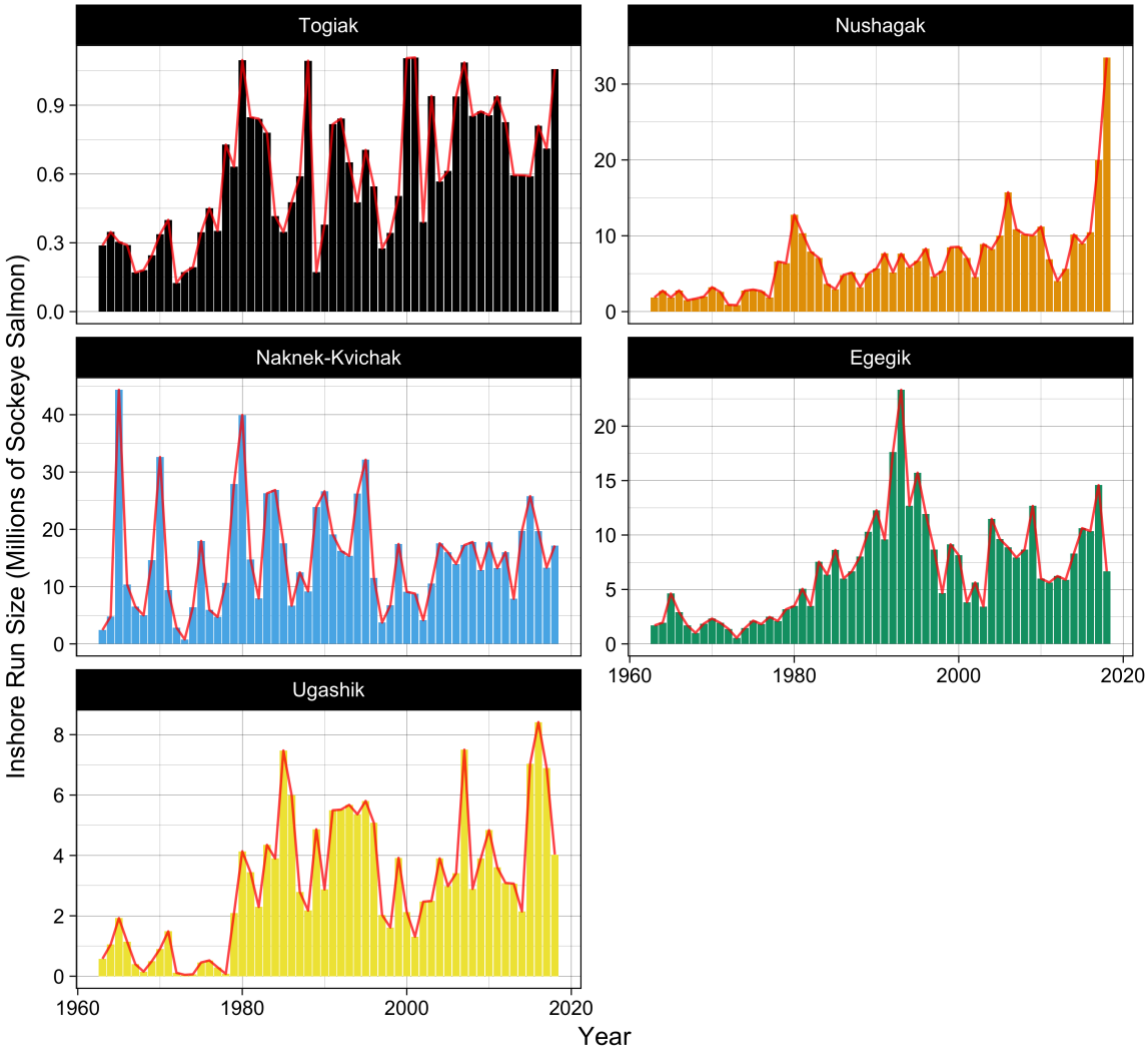

Figure R13-25. Annual Bristol Bay sockeye salmon inshore run size by commercial fishing district (1963-2018).

7.6. Togiak Herring Population Trends

Contributed by: Greg Buck and Sherri Dressel
Alaska Department of Fish and Game

Methods: The biomass of mature Pacific herring (*Clupea pallasii*) occurring in the Togiak District of Bristol Bay has been tracked through aerial surveys since the late 1970s using methods described by Lebida and Whitmore (1985). An age-structured analysis (ASA)

model is used to forecast herring biomass in Togiak District of Bristol Bay. The data used in the ASA model includes aerial survey estimates of mature biomass weighted by a confidence score, age composition and weight-at-age information collected from the fishery, and harvest from both the seine and gillnet fisheries. Recruitment of Togiak herring to the fishery begins around age-4 and fish are believed to be fully recruited into the fishery around age-8.

Trends (Figure R13-26 & 27): Togiak mature herring biomass as estimated by the ASA model increased from a low of 63,149 short tons in 1980 to over 430,000 short tons from 1985 to 1987, due to large age-4 recruitments in 1981 and 1982 . The biomass then declined through the mid-1990s and has remained stable since that time. Model estimated mature biomass increased gradually from 122,903 short tons in 2009 to 216,418 short tons in 2013 and then decreased slightly from 209,824 short tons in 2014 through 179,635 short tons in 2016. Due to budget constraints and poor weather for aerial surveys, there were no aerial survey estimates used in the model for 2016-2018, increasing the uncertainty in model-estimated mature biomass for those years and in the 2019 forecast. Without survey biomass data from 2016-2018, biomass and recruitment estimate from 2016 to 2018, as well as the forecast biomass, depend on aerial survey biomass estimates prior to 2016 and age composition samples through 2018. The 2019 forecast is the highest forecast since 1993 due to the large proportion of young (age-4 and age-5 fish) observed in the commercial purse seine samples in 2018 and the resultant large recruitment estimates for 2017 and 2018 (Figure R13-27)).

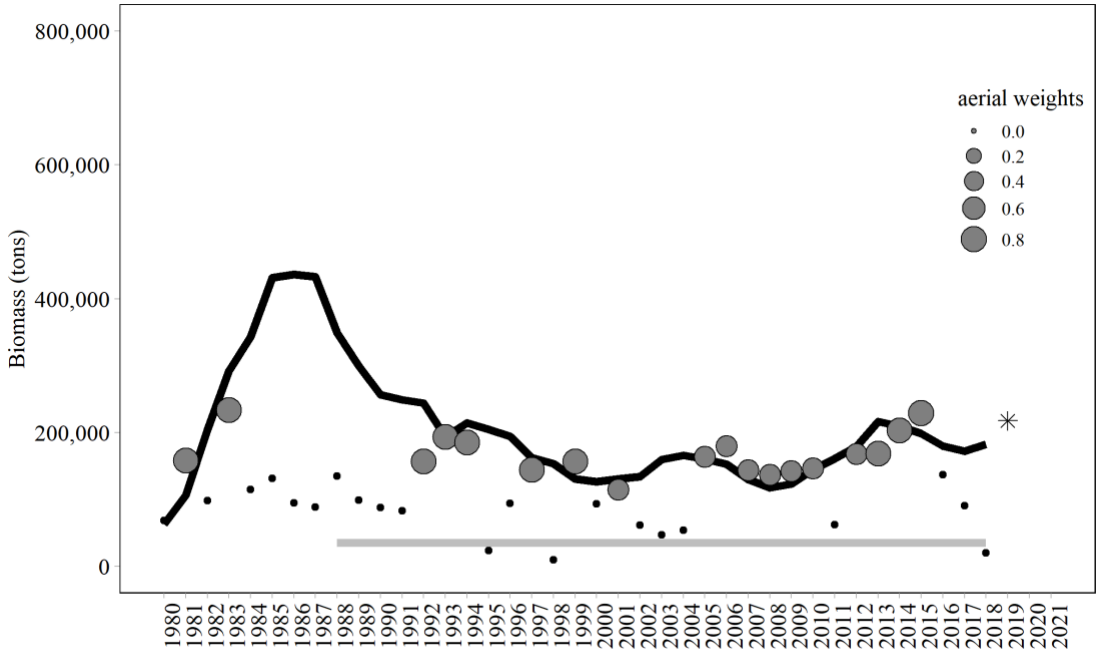

Figure R13-26. Aerial survey-estimated biomass plus pre-peak catch (grey points), model-estimated mature biomass (black solid line), model-estimated mature biomass forecast (black star), and biomass threshold below which fishing is not allowed (grey line). The size of the grey points reflects the confidence weighting of each aerial survey estimate in the model based on weather, number of surveys, quality of surveys, and timing of surveys relative to the spawn (ranging from 0=no confidence to 1=perfect confidence).

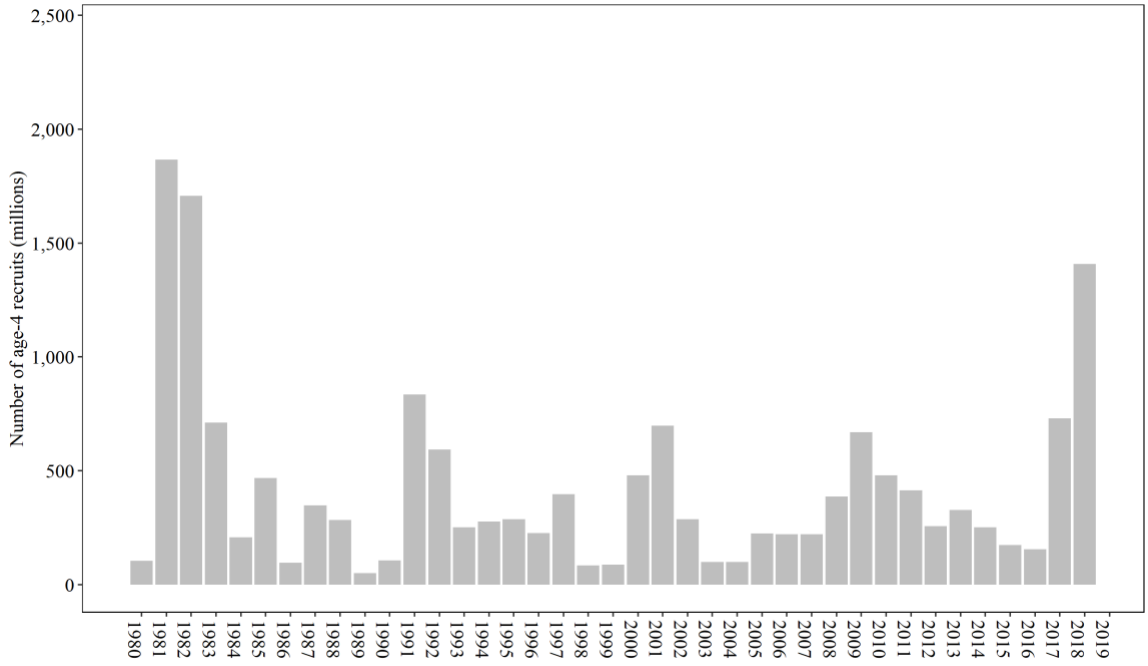

Figure R13-27. Model estimates of Togiak herring age-4 recruit strength (numbers of age-4 mature and immature herring).

7.7. Eastern Bering Sea Commercial Crab Stock Biomass Indices

Contributed by Robert Foy, Christie Lang, Jon Richar
Kodiak Laboratory, Alaska Fisheries Science Center, National Marine Fisheries Service, NOAA, Kodiak, AK

Methods: This indicator is the commercial crab species biomass time series in the eastern Bering Sea. The eastern Bering Sea bottom trawl survey has been conducted annually since 1975; the purpose of the survey is to collect data on the distribution and abundance of crab, groundfish, and other benthic resources in the eastern Bering Sea. The data provided here include the time series of 1998 to 2018. The trends in crab biomass may be indicative of trends in benthic production or benthic response to environmental variability. The commercial crab biomass also indicates trends in exploited resources over time.

Trends (Figure R13-28): The historical trends of commercial crab biomass and abundance are highly variable. In 2018, there was an overall decrease in biomass and abundance in red king, blue king, and Tanner crab stocks. Bristol Bay red king crab mature males declined by 43% against overall mean in 2018, by 71% since 2014 and reaching a 35-year low. Bristol Bay red king crab mature females also declined 53% in 2018 reaching a 22-year low. The St. Matthew blue king crab adult male stock continued a four-year decline since 2014 to the lowest levels observed for this stock in 2018. Female blue king crab biomass is not adequately sampled during this survey due to a nearshore distribution around St. Matthew Island. Tanner crab male and female biomass declined by 20 and 30%, respectively, in 2018 due mostly to declines in the eastern

portion of the stock. The declining trend has continued since 2014. The western portion of the stock, however, has been increasing or stable in recent years. The snow crab stock biomass increased in 2018 with a 60% increase in mature females. The stock had declined to all-time lows in 2016 but increased recruitment has led to an increase that is expected to continue. Pribilof Islands crab stocks remain extremely depressed with variable survey biomass due to trawl survey limitations due to habitat and the contagious crab distribution.

Figure R13-28. Historical biomass for commercial crab stocks caught on the Eastern Bering Sea bottom trawl surveys (1998-2018). Broken and solid green lines indicate overall mean and 1 x standard deviation. Symbols on right side indicate 2014-2018 trend and extent of the 2014-2018 mean relative to the 1998-2018 mean.

8. Benthos

8.1. Miscellaneous Species on the Eastern Bering Sea Shelf

Contributed by Robert Lauth and Elizabeth Dawson
NOAA - Alaska Fisheries Science Center

Methods: “Miscellaneous” species fall into three groups: eelpouts (Zoarcidae), poachers (Agonidae), and sea stars (Asteroidea). The three species comprising the eelpout group are the wattled eelpout (*Lycodes palearis*), shortfin eelpout (*L. brevipes*) and to a lesser extent the marbled eelpout (*L. raridens*). The biomass of poachers is dominated by the sturgeon poacher (*Podothecus acipenserinus*) and to a lesser extent the sawback poacher (*Leptagonus frenatus*). The composition of sea stars in shelf trawl catches are dominated by the purple-orange sea star (*Asterias amurensis*), which is found primarily in the inner/middle shelf regions, and the common mud star (*Ctenodiscus crispatus*), which is primarily an inhabitant of the outer shelf. Relative Catch-Per-Unit-Effort (CPUE) by weight was calculated and plotted for each species or species group by year for 1982-2018. Relative CPUE was calculated by setting the largest biomass in the time series to a value of 1 and scaling other annual values proportionally. The standard error (±1) was weighted proportionally to the CPUE to produce a relative standard error.

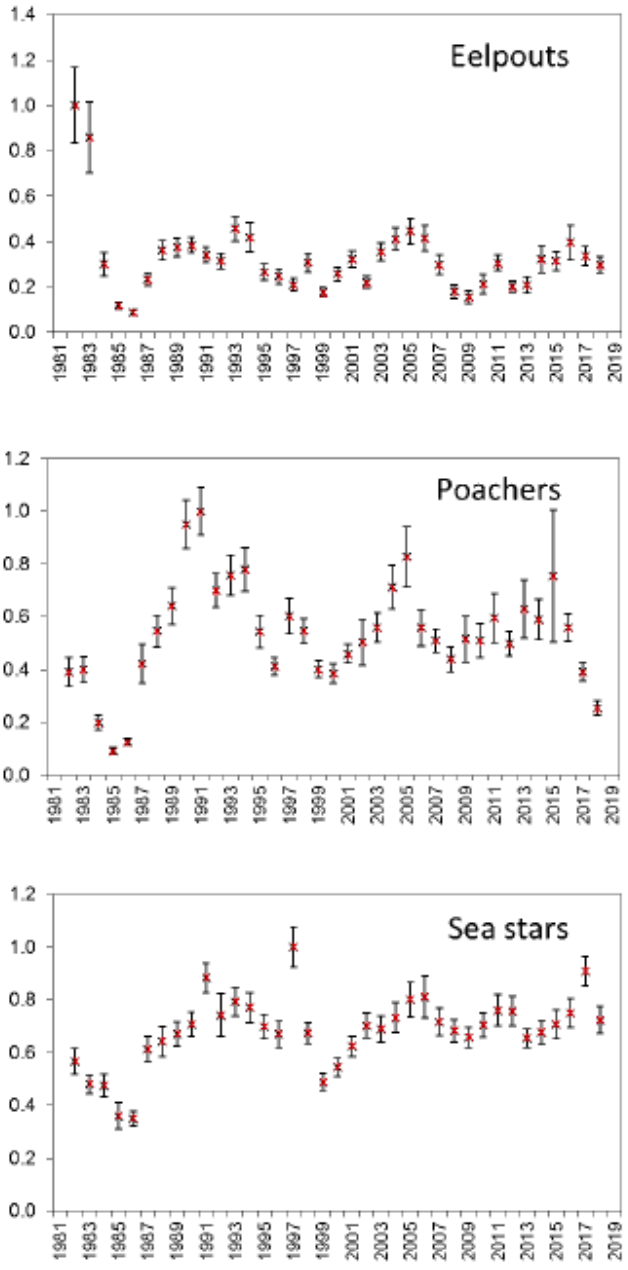

Trends R13-29: The 2018 relative CPUE for eelpouts decreased by 12% from 2017, but the 2018 estimate was just above the average of the estimates over the last 10 years. The poacher group CPUE decreased by 36% since 2017, by 55% since 2016, and by 66% since 2015. The 2018 poacher estimate ranked as the lowest since 1987. Only during a single three year time period from 1984 to 1986, were poacher estimates lower than in 2018. The sea stars as a group decreased by 20% from 2017 to 2018, and the 2018 CPUE was just below the CPUE average of the last 10 years.

Figure R13-29. Eastern Bering Sea shelf bottom trawl survey relative CPUE (max biomass = 1.0) for miscellaneous fish species during May to August from 1982-2018. Error bars indicate standard error (±1).

9. Biogenic Habitat

Note: There was one ETSO submitted, but the investigator noted that the data were not a good indicator of trends, so we chose not to include it in here.

10. Marine Birds

10.1. Seabird Monitoring Summary from Alaska Maritime National Wildlife Refuge

Contributed by Marc Romano and Heather Renner
Alaska Maritime National Wildlife Refuge, 95 Sterling Highway, Suite 1, Homer, AK 99603

Methods: The Alaska Maritime National Wildlife Refuge has monitored seabirds at colonies around Alaska in most years since the early- to mid-1970s. Time series of annual breeding success and phenology (among other parameters) are available from over a dozen species at eight Refuge sites in the Gulf of Alaska, Aleutian Islands, and Bering and Chukchi Seas. Monitored colonies in the eastern Bering Sea include St. Paul and St. George Islands. Here, we focus on cliff-nesting, primarily fish-eating species: black-legged kittiwake (*Rissa tridactyla*), red-legged kittwake (*R. brevirostris*), common murre (*Uria aalge*), thick-billed murre (*U. lomvia*), and red-faced cormorants (*Phalacrocorax urile*). Reproductive success is defined as the proportion of nest sites with eggs (or just eggs for murres, as they do not build nests) that fledged a chick.

Trends Figure R13-30: Both kittiwake species and red-faced cormorants showed overall poor reproductive success in 2018 at both St. Paul and St. George Islands. This was the fourth consecutive year of poor reproductive performance for both black-legged and red-legged kittiwakes. For 2009-2014 mean kittiwake reproductive success in the Pribilof Islands was considerably higher than 2015-2018 (0.30 vs. 0.03 respectively, for both species and both islands combined). Thick-billed murres and common murres monitored in the Pribilof Islands had reproductive success during 2018 (0.42 for both species combined) that was comparable to the long-term mean (0.39) but far fewer birds than usual attended the colony. As a result, total production of murre chicks for both colonies was likely low when compared to years when a greater number of birds attempt to breed. Despite the relatively good reproductive success for murres in 2018, mean reproductive success for both species on both islands was higher for 2009-2014 (0.49) than for 2015-2018 (0.25). Mean hatching dates were late for kittiwakes and murres that successfully hatched chicks in 2018. This later than average hatch dates for murres and kittiwakes continued for 2015-2018 when compared to hatch dates for 2009-2014.

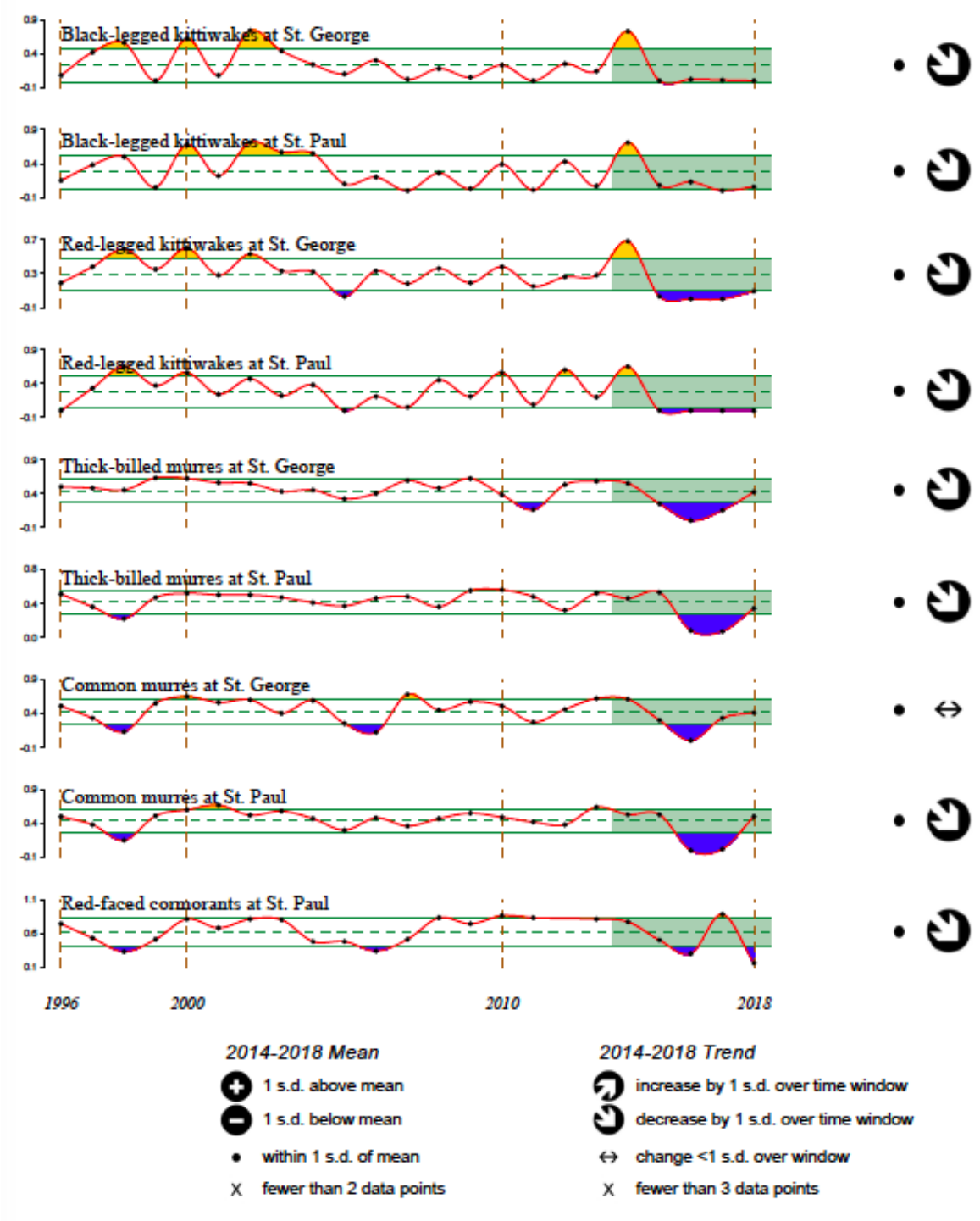

Figure R13-30. Reproductive success of five seabird species at St. George and St. Paul Islands between 1996-2018. Broken and solid green lines incidate overall mean and 1 x standard deviation. Symbols on right side indicate 2014-2018 trend and extent of the 2014-2018 mean relative to the 1996-2018 mean.

11. Marine mammals

11.1. Northern Fur Seal (*Callorhinus ursinus*) Pup Production in the Bering Sea

Contributed by Rod Towell, Rolf Ream, John Bengtson, Michael Williams, and Jeremy Sterling
NOAA - Alaska Fisheries Science Center, Marine Mammal Laboratory

Methods: Northern fur seals were listed as depleted under the Marine Mammal Protection Act (MMPA) in 1988 because population levels had declined to less than 50% of levels observed in the late 1950s, with no compelling evidence that carrying capacity had changed (NMFS, 2007). Fisheries regulations were implemented in 1994 (50 CFR 679.22(a) (6)) to create a Pribilof Islands Area Habitat Conservation Zone (no fishing with trawl permitted), in part to protect northern fur seals. Under the MMPA, this stock remains listed as “depleted" until population levels reach at least the lower limit of its optimum sustainable population (estimated at 60% of carrying capacity). A Conservation Plan for the northern fur seal was written to delineate reasonable actions to protect the species (NMFS, 2007). Pup production of northern fur seals on Pribilof and Bogoslof Islands is estimated by the Marine Mammal Laboratory biennially using a mark recapture method (shear-sampling) on 1-2 month old pups. The most recent pup production estimate for the Pribilof Islands was conducted during August 2018; pup production on Bogoslof Island was assessed in August 2015.

Trends(R13-31): An estimated 75,719 (SE = 1,008) fur seal pups were born on St. Paul Island and an estimated 21,625 (SE = 345) fur seal pups were born on St. George Island in 2018. The 2018 estimated production for St. Paul Island is approximately 6.1% less than the 2016 estimate. The St. George estimate is approximately 5.5% greater in 2018 than 2016. From 2009 to 2016 pup production shows and insignificant decrease (P = 0.17) of approximately 2.53% per year on St. Paul Island and an insignificant increase (P = 0.28) of approximately 3.27% per year St. George Island. Using the draft estimates for 2018, pup production has been declining since 1998 at an approximate annual rate of 4.0% on St. Paul Island and shows no significant trend on St. George Island over the same time period. Since 2002, pup production has been lower than was estimated in 1921 on St. Paul Island and in 1919 on St. George Island, when the populations were recovering at 8% annually from a pelagic harvest that ended in the early 20th century. On a positive note, St. George Island pup production has shown an increase for three consecutive estimates over a 6 year period. Bogoslof Island pup production has continued an increasing trend since the first pup observation in 1980. Estimated pup production has increased at an annual rate of 10.1% (SE = 1.08) from 1997 to 2015.

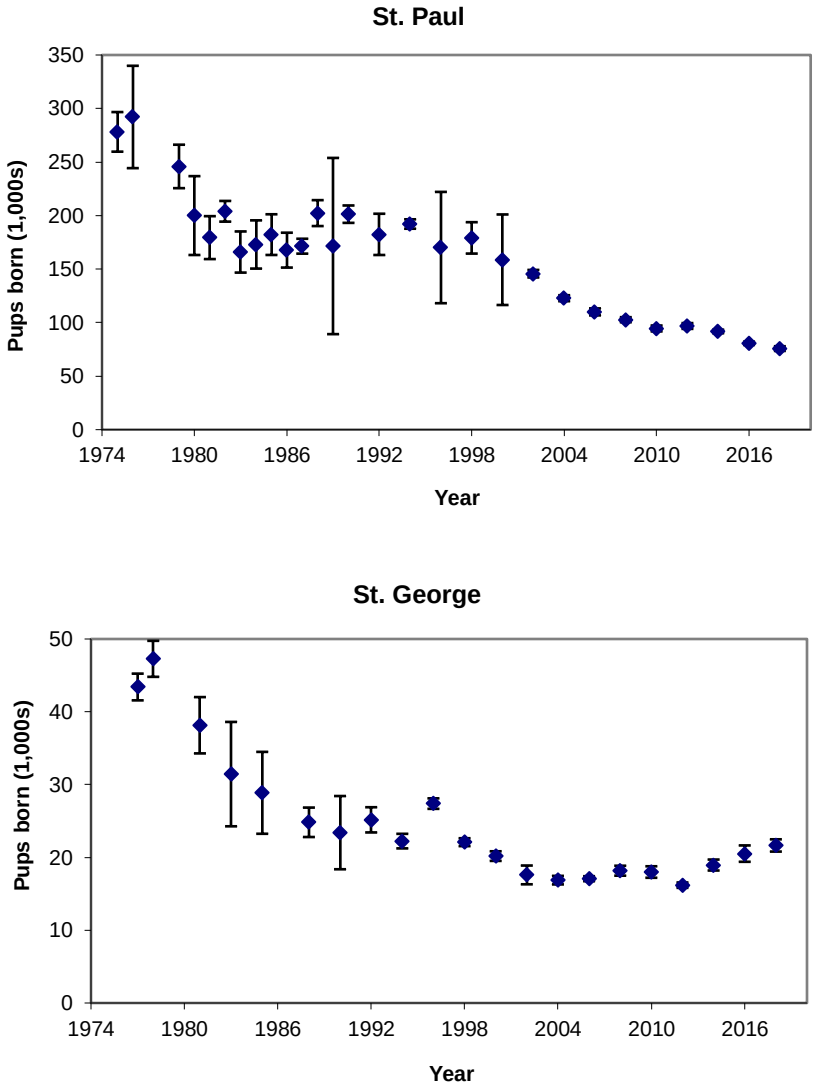

Figure R13-31. Estimated number of northern fur seal pups born on St. Paul Island and St. George Island in the Pribilof Islands 1975-2018. Error bars are approximate 95% confidence intervals. Note that St. Paul Island estimates do not include pups born on Sea Lion Rock.

References

Batten, S.D., Clarke, R.A., Flinkman, J., Hays, G.C., John, E.H., John, A.W.G., Jonas, T.J., Lindley, J.A., Stevens, D.P., and Walne, A.W. (2003) CPR sampling – The technical background, materials and methods, consistency and comparability. Progress in Oceanography, 58, 193-215.

Boldt, J. L., & Haldorson, L. J. (2004). Size and condition of wild and hatchery pink salmon juveniles in Prince William Sound, Alaska. *Transactions of the American Fisheries Society*, *133*(1), 173-184.

Brodeur, R. D., Fisher, J. P., Teel, D. J., Emmett, R. L., Casillas, E., & Miller, T. W. (2004). Juvenile salmonid distribution, growth, condition, origin, and environmental and species associations in the Northern California Current.

Chiba, S., E. Di Lorenzo, A. Davis, J. E. Keister, B. Taguchi, Y. Sasai, and H. Sugisaki (2013) Large-scale climate control of zooplankton transport and biogeography in the Kuroshio-Oyashio Extension region, Geophys. Res. Lett., 40, 5182–5187, doi:10.1002/grl.50999.

Di Lorenzo, E., Schneider, N., Cobb, K. M., Franks, P. J. S., Chhak, K., Miller, A. J., ... & Rivière, P. (2008). North Pacific Gyre Oscillation links ocean climate and ecosystem change. *Geophysical research letters*, *35*(8).

Eisner, L., Siddon, E., Strasburger, W. (2015) Spatial and temporal changes in assemblage structure of zooplankton and pelagic fish across varying climate conditions in the eastern Bering Sea. Izvestia TINRO, vol 181, 141-160.

Elison, T. B., Schaberg, K. L., & Bergstrom, D. J. (2012). *Kuskokwim River Salmon Stock Status and Kuskokwim Area Fisheries, 2012: A Report to the Alaska Board of Fisheries*. Alaska Department of Fish and Game, Division of Sport Fish, Research and Technical Services.

Hunt Jr, G. L., Ressler, P. H., Gibson, G. A., De Robertis, A., Aydin, K., Sigler et al. (2016) Euphausiids in the eastern Bering Sea: A synthesis of recent studies of euphausiid production, consumption and population control. *Deep Sea Research Part II: Topical Studies in Oceanography*, *134*, 204-222.

Iida T., S.I. Saitoh, T. Miyamura, M. Tortani, H. Fukushima, and N. Shiga (2002). Temporal and spatial variability of coccolithophore blooms in the eastern Bering Sea, 1998–2001. Prog. Oceanogr. 55: 165–175.

Iida, T., Mizobata, K., & Saitoh, S. I. (2012). Interannual variability of coccolithophore Emiliania huxleyi blooms in response to changes in water column stability in the eastern Bering Sea. *Continental Shelf Research*, *34*, 7-17.

Ladd C., Stabeno, P.J. (2012) Stratification on the Eastern Bering Sea shelf revisited. Deep Sea Res. II 65-70, 72-83.

Lebida R. C. and D. C. Whitmore. (1985) Bering Sea Herring Aerial Survey Manual. Bristol Bay Data Report No. 85-2, Alaska Department of Fish and Game, Anchorage, AK.

Mantua, N.J., S.R. Hare, Y. Zhang, J.M. Wallace, and R.C. Francis (1997) A Pacific interdecadal climate oscillation with impacts on salmon production. Bull. Amer. Meteor. Soc., 78, pp. 1069-1079.

Newman, M. and Co-Authors (2016) The Pacific Decadal Oscillation, Revisited. J. Climate, doi.org/10.1175/JCLI-D-150508.1

Olson, M. B., & Strom, S. L. (2002). Phytoplankton growth, microzooplankton herbivory and community structure in the southeast Bering Sea: insight into the formation and temporal persistence of an Emiliania huxleyi bloom. *Deep Sea Research Part II: Topical Studies in Oceanography*, *49*(26), 5969-5990.

Ortiz, I,. Wiese, F., Greig, A., (2012) Marine regions boundary data for the Bering Sea shelf and slope. UCAR/NCAR - Earth Observing Laboratory/Computing, Data, and Software Facility. Dataset. doi:10.5065/D6DF6P6C.

Paul, A. J., Paul, J. M., & Smith, R. L. (1998). Seasonal changes in whole-body energy content and estimated consumption rates of age 0 walleye pollock from Prince William Sound, Alaska. *Estuarine, Coastal and Shelf Science*, *47*(3), 251-259.

Parsons, T.R., Maita, Y., Lalli, C.M. (1984) A Manual of Chemical and Biological Methods for Seawater Analysis. Pergamon Press, Oxford, England, 173 pp.

Petitgas, P. (1993). Geostatistics for fish stock assessments: a review and an acoustic application. *ICES Journal of Marine Science*, *50*(3), 285-298.

Simpson, J. H., C. M. Allen, and N. C. G. Morris (1978) Fronts on the continental shelf, J. Geophys. Res., 83(C9), 4607-4614.

Smith, J. N., Ressler, P. H., & Warren, J. D. (2013). A distorted wave Born approximation target strength model for Bering Sea euphausiids. *ICES Journal of Marine Science*, *70*(1), 204-214.

Thorson, J.T., A.O. Shelton, E.J. Ward, and H.J. Skaug. (2015) Geostatistical delta-generalized linear mixed models improve precision for estimated abundance indices for West Coast groundfishes. ICES Journal of Marine Science 72(5):1297-1310. doi:10.1093/icesjms/fsu243

Thorson, J.T., and K. Kristensen, K. (2016) Implementing a generic method for bias correction in statistical models using random effects, with spatial and population dynamics examples. Fisheries Research 175:66-74. doi:10.1016/j.fishres.2015.11.016. url: http://www.sciencedirect.com/science/article/pii/S0165783615301399

Thorson, J.T., M.L. Pinsky, and E.J. Ward. (2016a) Model-based inference for estimating shifts in species distribution, area occupied and centre of gravity. Methods in Ecology and Evolution 7(8):990-1002.

Thorson, J.T., A. Rindorf, J. Gao, D.H. Hanselman, and H. Winker. (2016b) Density-dependent changes in effective area occupied for sea-bottom-associated marine fishes. Proceedings of the Royal Society B 283(1840):20161853.

Trenberth, K.E. and J.W. Hurrell (1994) Decadal Atmospheric-Ocean Variations in the Pacific. Climate Dynamics, 9, 303-319, doi.org/10.1007/BF00204745

Watson JT. (2019) Spatial and temporal visualizations of satellite-derived sea surface temperatures for Alaska fishery management areas. Pacific States e-Journal of Scientific Visualizations. Article 003. doi: 10.28966/PSESV.2019.003